Mon. Not. R. Astron. Soc. **399,** 239–263 (2009) doi:10.1111/j.1365-2966.2009.15244.x

Temperature and abundance profiles of hot gas in galaxy groups – II. Implications for feedback and ICM enrichment

Jesper Rasmussen[1]★† and Trevor J. Ponman[2]

[1]*Carnegie Observatories, 813 Santa Barbara Street, Pasadena, CA 91101, USA*
[2]*School of Physics and Astronomy, University of Birmingham, Edgbaston, Birmingham B15 2TT*

Accepted 2009 June 12. Received 2009 June 10; in original form 2009 February 16

ABSTRACT

We investigate the history of galactic feedback and chemical enrichment within a sample of 15 X-ray bright groups of galaxies, on the basis of the inferred Fe and Si distributions in the hot gas and the associated metal masses produced by core-collapse and Type Ia supernovae (SNe). Most of these cool-core groups show a central Fe and Si excess, which can be explained by prolonged enrichment by SN Ia and stellar winds in the central early-type galaxy alone, but with tentative evidence for additional processes contributing to core enrichment in hotter groups. Inferred metal mass-to-light ratios inside r_{500} show a positive correlation with total group mass but are generally significantly lower than in clusters, due to a combination of lower global intracluster medium (ICM) abundances and gas-to-light ratios in groups. This metal deficiency is present for products from both SN Ia and SN II, and suggests that metals were either synthesized, released from galaxies or retained within the ICM less efficiently in lower mass systems. We explore possible causes, including variations in galaxy formation and metal release efficiency, cooling out of metals, and gas and metal loss via active galactic nuclei (AGN) – or starburst-driven galactic winds from groups or their precursor filaments. Loss of enriched material from filaments coupled with post-collapse AGN feedback emerges as viable explanations, but we also find evidence for metals to have been released less efficiently from galaxies in cooler groups and for the ICM in these to appear chemically less evolved, possibly reflecting more extended star formation histories in less massive systems. Some implications for the hierarchical growth of clusters from groups are briefly discussed.

Key words: galaxies: clusters: general – galaxies: evolution – intergalactic medium – X-rays: galaxies: clusters.

1 INTRODUCTION

Groups of galaxies are repositories for a substantial fraction of all baryons and metals at low redshift. Being much more numerous than more massive clusters and more susceptible to the effects of non-gravitational processes such as galaxy winds driven by supernovae (SNe) or active galactic nuclei (AGN; e.g. Helsdon & Ponman 2000; Borgani et al. 2004; Romeo et al. 2006), they represent unique laboratories for the study of galactic feedback and chemical enrichment of the intergalactic medium. In practice, this can be exploited through X-ray observations of the hot intragroup gas, which allow the abundance of several heavy elements in this gas to be constrained.

Numerous such studies have been undertaken for massive galaxy clusters, providing a reasonably well-constrained picture of the amount and distribution of metals in the intracluster medium (ICM) and in the cluster galaxies themselves (Finoguenov, David & Ponman 2000; Böhringer et al. 2004; De Grandi et al. 2004; Mouhcine et al. 2006; Baldi et al. 2007; Leccardi & Molendi 2008). However, despite extensive observational and theoretical efforts, several important questions related to ICM enrichment still remain, such as the relative importance of the mechanisms responsible for transferring metals from galaxies to the ICM, and the role of mergers and galactic wind activity in redistributing enriched material. For example, it has been notoriously difficult to reproduce observed ICM metal distributions in cosmological hydrodynamical simulations of clusters, suggesting that important processes affecting baryons in these systems may still be inadequately captured or altogether missing in such models (see e.g. review by Borgani et al. 2008b). Characterization of the chemical makeup of the hot gas in more numerous lower mass groups could provide an important ingredient in resolving these questions. Due to the structural role played by groups in connecting the 'field' – i.e. isolated galaxies and the intergalactic medium – with the rare high-density peaks

★E-mail: jr@ociw.edu
†Chandra Fellow.

represented by massive clusters, a clearer picture of enrichment in groups may have ramifications for our understanding of the evolution of baryons across a wide range of environments.

In an early study of the distribution of elemental abundances in intragroup gas, Finoguenov & Ponman (1999) investigated three groups, for which they found significant spatial variations in the ratio of iron to α-element abundances, concluding that both SNe Type Ia and II must have contributed to the enrichment of the ICM in groups. Evidence for significant iron gradients in a sample of 10 groups and early-type galaxies were also found from *ROSAT* data by Buote (2000b). Finoguenov, Arnaud & David (2001) followed this up using a larger sample of 18 cool clusters, but with only two systems at $T < 2$ keV, while Finoguenov et al. (2002) studied nine groups mainly in the context of their entropy profiles and the constraints they imposed on preheating scenarios. More recent work include the two-dimensional *XMM–Newton* results of Finoguenov et al. (2006, 2007), but the main focus here was the entropy and pressure structure of the ICM. Thus, while most of these studies have focused on $T \lesssim 2$ keV systems, detailed discussions of the abundance distributions and the implications for galaxy and group evolution have generally been limited and based on samples of just a few groups (e.g. Finoguenov & Ponman 1999). Hence, a dedicated study of chemical enrichment in a substantial number of groups has been lacking.

In the first paper in this series (Rasmussen & Ponman 2007, hereafter Paper I), we presented projected radial profiles of temperature and Fe and Si abundance of the hot intragroup gas in a sample of 15 groups, discussing the results in a statistical framework. The groups were selected mainly from the Group Evolution Multiwavelength Study (GEMS) sample of Osmond & Ponman (2004), on the basis of their good photon statistics in available *Chandra* data and for their relatively undisturbed X-ray morphology. The low *Chandra* background enabled robust abundance constraints to reasonably large radii, with the majority of our groups having Fe and Si profiles extracted to at least $2/3\ r_{500}$, where r_{500} is the radius enclosing a mean density of 500 times the critical density. At the same time, the spatial resolution of *Chandra* allowed sampling of group cores at a level of detail usually unattainable with other X-ray telescopes. With only one exception (NGC 4125), all the groups were found to contain cooler gas in the central regions. Main results of the study included the discovery that Fe abundances in the groups show a highly significant decrease with radius, declining continually from a central excess towards a value at r_{500} which is, on average, lower than corresponding values seen in more massive clusters by a factor of 2. In addition, it was found that Fe enrichment in group cores is dominated by SN Ia as also found for more massive clusters (e.g. De Grandi et al. 2004), thus confirming early, tentative *ASCA* results (Finoguenov et al. 2000). The SN II contribution to enrichment increases with radius, however, and potentially becomes exclusive at radii approaching r_{500}.

The purpose of this paper is to explore some of the implications of these results. In Section 2, we outline the derivation of gas and metal masses and the optical properties of the groups. Section 3 presents the main results inferred from these quantities and from the observed abundance distributions, including the metal masses produced by SN Ia and SN II, the corresponding mass-to-light ratios, and the impact of SN in the brightest group galaxy (BGG) and in the groups as a whole. One finding is that the metal mass-to-light ratios deviate substantially from results for more massive systems, and we explore a variety of possible explanations for this in Section 4, along with some further implications for the feedback and chemical enrichment history of the groups in Section 5. Section 6 briefly discusses and summarizes the results, including some general implications for structure formation.

As in Paper I, we use the solar abundance table of Grevesse & Sauval (1998), theoretical supernova yields from Iwamoto et al. (1999) and Nomoto et al. (2006), and the Kendall rank–order correlation coefficient τ to quantify the significance σ_K of linear relationships. A value of $H_0 = 70$ km s^{-1} Mpc^{-1} is assumed throughout, and all errors are given at the 68 per cent confidence level unless otherwise stated.

2 METAL MASSES AND OPTICAL LUMINOSITIES WITHIN r_{500}

Results from Paper I for the abundance profiles are summarized in Fig. 1. The data points here are similar to those of fig. 11 in Paper I, showing the results in radial bins of 20 measurements each. We briefly recapitulate the distinct features of these profiles, which are (i) a central abundance excess for both Fe and Si, often accompanied by a dip in the very centre for both elements and (ii) a clear decline in Fe abundance with radius towards a value of $\sim$0.1 $Z_\odot$ at r_{500}, with a somewhat less pronounced decline for Si (which furthermore flattens out or even rises at large radii). For reference, the SN yields adopted here, as explained in Paper I, are $M_{\rm Fe} \approx 0.79\,{\rm M}_\odot$ and $M_{\rm Si} \approx 0.21\,{\rm M}_\odot$ for Fe and Si from SN Ia, and $M_{\rm Fe} \approx 0.08\,{\rm M}_\odot$ and $M_{\rm Si} \approx 0.12\,{\rm M}_\odot$ for core-collapse SNe including SN II. This implies $Z_{\rm Si}/Z_{\rm Fe} \approx 0.46\,Z_{{\rm Si},\odot}/Z_{{\rm Fe},\odot}$ for SN Ia ejecta, $2.62\,Z_{{\rm Si},\odot}/Z_{{\rm Fe},\odot}$ for those of SN II, and with a solar abundance ratio requiring 3.4 SN II per SN Ia. The impact of assuming different sets of SN yields will be discussed in Section 3.

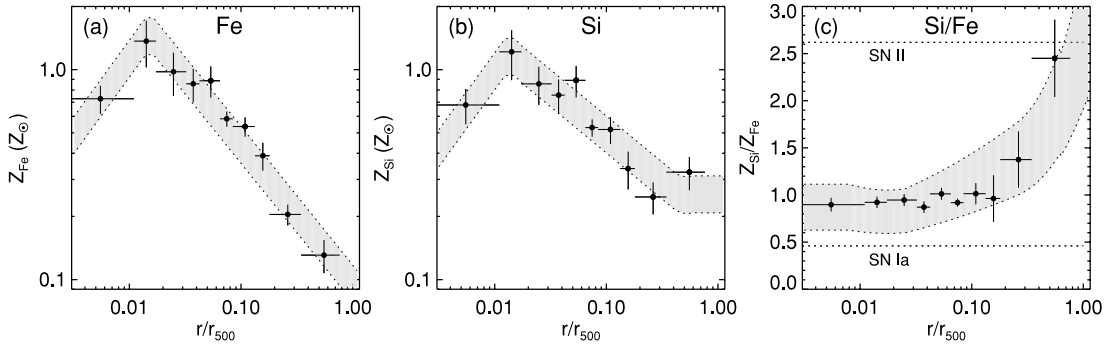

Figure 1. Fe and Si abundance profiles for all groups, in radial bins of 20 data points, along with the corresponding Si/Fe ratios. Shaded areas illustrate the adopted 1σ error envelopes on our parametrized abundance profiles. Dotted lines in (c) show the expectations for pure SN Ia and SN II enrichment.

2.1 Parametrizing the abundance profiles

For the majority of our groups, abundances could not be measured all the way out to r_{500}. In order to enable predictions of $Z(r)$ beyond the radius of measurement for individual groups, as well as to facilitate visualization of sample-averaged results, we made parametrizations of the average abundance profiles in Fig. 1. This approach can be justified on the grounds that while the statistical uncertainties on $Z_{\rm Fe}$ and $Z_{\rm Si}$ can be quite large for individual groups, the intrinsic scatter in these quantities is reasonably small outside the innermost regions. Outside the peak of the profiles in Fig. 1, we have adopted the fitted relations of Paper I (equations 8 and 9) for these parametrizations. Inside the peaks, a linear rise in $\log Z$ versus $\log(r/r_{500})$ has been assumed, normalized such as to ensure a continuous behaviour at the peaks. Outside $r = 0.1r_{500}$, where the vast majority of gas resides, the typical standard error on the mean in the individual bins in Figs 1(a) and (b) is 16 per cent for $Z_{\rm Fe}$ and 18 per cent for $Z_{\rm Si}$. We have conservatively adopted 20 per cent relative errors as representative for our parametrizations of both profiles. These 20 per cent error envelopes are shown as shaded regions in Fig. 1; within these errors, the parametrizations are consistent with every data point in the figure. Note that the shaded region in Fig. 1(c) is not a direct parametrization of the Si/Fe ratios, but results from the ratio of the parametrized Si and Fe profiles, with their adopted errors added in quadrature.

Unless otherwise stated, our analysis employs the observed abundance profiles of individual groups out to the edge of the usable *Chandra* data, extrapolating these to larger radii where necessary using the above parametrizations and their associated errors. Though obviously a model-dependent approach, the adopted parametrizations are at least empirically motivated across all radii considered here, and the resulting Si/Fe ratios remain consistent with commonly used SN model yields everywhere inside r_{500}. Furthermore, as will be demonstrated, there is no clear evidence for the observed abundance profiles at large radii to be systematically different for, for example, high-and low-temperature groups, so the adopted parametrizations should be reasonably representative for the entire group sample. The additional precaution of adopting conservative errors on these was taken to further alleviate concerns regarding this approach.

2.2 Derivation of gas and metal masses

For the calculation of gas and metal masses of the groups, we adopted a standard one-dimensional β-model to describe the gas density profiles, using values of β and $r_{\rm c}$ for each group taken from the literature. These values are listed in Table 1, taken from the *ROSAT* analyses of Mulchaey et al. (2003) for NGC 507, NGC 4125 and NGC 7619, Davis et al. (1996) for NGC 2300 and Osmond & Ponman (2004) for the remainder.

The gas density profile of each group was normalized by means of the measured *Chandra* flux in the 0.1–0.3 r_{500} range, using the spectral normalization A from XSPEC,

$$A = \frac{10^{-14}}{4\pi D^2(1+z)^2}\int_{0.1r_{500}}^{0.3r_{500}} n_{\rm e}n_{\rm H}{\rm d}V\,{\rm cm}^{-5}, \quad (1)$$

where D is the group distance (from Paper I) and $n_{\rm e}$ and $n_{\rm H}$ are the number densities of electrons and hydrogen atoms, respectively. The reason for normalizing the profiles using the flux outside $r = 0.1r_{500}$ is that many of the published gas density parameters result from two-component fits, with one component used to describe the emission in and around the central galaxy, and the other, of interest here, to describe the extended group emission. This approach also reduces the impact of projection effects on the resulting normalizations, and suppresses effects related to blurring by the *ROSAT* point spread function. Where relevant, a geometric correction was applied to A, to account for the lost detector area due to removed point sources and incomplete azimuthal coverage of the relevant radial range (see Paper I for details). The median correction factor was 1.38, with no significant dependence on, for example, mean group temperature. Gas and metal masses were then calculated using the adopted β-model parameters. Errors on these masses within the radius of interest were obtained on the basis of 5000 Monte Carlo realizations of the gas density and abundance profiles of each group. For each realization, gas density parameters (A, β, $r_{\rm c}$)

Table 1. Gas density parameters, gas and metal masses, optical and near-infrared luminosities, and galaxy velocity dispersions for the sample, all obtained inside r_{500}. Also listed is the corresponding fractional metal mass $f_{\rm Ia}$ provided by SN Ia for both Fe and Si.

Group	$\langle T_{\rm X}\rangle$ (keV)	β	$r_{\rm c}$ (kpc)	$M_{\rm gas}$ ($10^{12}\,{\rm M}_\odot$)	$M_{\rm Fe}$ ($10^{8}\,{\rm M}_\odot$)	$f_{\rm Ia}$ (Fe)	$M_{\rm Si}$ ($10^{8}\,{\rm M}_\odot$)	$f_{\rm Ia}$ (Si)	$L_{\rm B}$ ($\log {\rm L}_\odot$)	$L_{\rm K}$ ($\log {\rm L}_\odot$)	σ_v (km s^{-1})
NGC 383	$1.65^{+0.04}_{-0.06}$	0.36 ± 0.00	2.1 ± 0.2	5.4 ± 0.1	18.4 ± 4.7	0.35	21.2 ± 7.9	0.08	11.50	12.26	450
NGC 507	$1.30^{+0.03}_{-0.03}$	0.42 ± 0.01	25.7 ± 0.6	3.9 ± 0.2	14.4 ± 3.9	0.31	16.4 ± 6.3	0.07	11.69	12.35	635
NGC 533	$1.22^{+0.05}_{-0.05}$	0.42 ± 0.01	2.2 ± 1.7	2.3 ± 0.1	5.0 ± 1.4	0.25	6.2 ± 2.7	0.06	11.47	12.11	439
NGC 741	$1.42^{+0.14}_{-0.12}$	0.44 ± 0.01	2.3 ± 0.2	2.7 ± 0.1	3.5 ± 1.3	0.34	11.9 ± 3.8	0.03	11.35	12.03	453
NGC 1407	$1.01^{+0.07}_{-0.09}$	0.46 ± 0.01	0.1 ± 0.1	0.7 ± 0.1	1.7 ± 0.3	0.31	2.0 ± 0.6	0.07	11.04	11.73	319
NGC 2300	$0.78^{+0.04}_{-0.03}$	0.41 ± 0.03	56.5 ± 16.8	1.2 ± 0.4	2.8 ± 1.0	0.19	3.8 ± 1.8	0.04	10.86	11.49	300
HCG 42	$0.80^{+0.05}_{-0.05}$	0.56 ± 0.02	4.7 ± 0.7	0.6 ± 0.1	1.2 ± 0.4	0.38	1.3 ± 0.6	0.10	11.32	11.92	282
MKW 4	$1.78^{+0.07}_{-0.09}$	0.43 ± 0.01	9.4 ± 2.9	7.0 ± 0.2	22.3 ± 6.6	0.54	19.7 ± 9.7	0.16	11.78	12.44	565
NGC 4125	$0.33^{+0.12}_{-0.05}$	0.47 ± 0.03	<0.7	0.2 ± 0.1	0.4 ± 0.1	0.27	0.6 ± 0.3	0.05	10.62	11.29	56
NGC 4325	$0.99^{+0.02}_{-0.02}$	0.58 ± 0.01	27.6 ± 5.0	1.8 ± 0.1	4.3 ± 1.4	0.71	2.8 ± 1.5	0.30	10.96	11.73	376
HCG 62	$1.00^{+0.03}_{-0.03}$	0.48 ± 0.01	2.4 ± 0.3	3.1 ± 0.1	5.3 ± 1.4	0.52	10.7 ± 3.5	0.06	11.35	12.02	418
NGC 5044	$1.12^{+0.03}_{-0.03}$	0.51 ± 0.00	6.0 ± 0.2	2.3 ± 0.1	6.3 ± 1.5	0.42	6.6 ± 2.0	0.10	11.22	11.92	426
NGC 5846	$0.66^{+0.04}_{-0.03}$	0.51 ± 0.01	2.2 ± 0.3	0.9 ± 0.1	2.1 ± 0.4	0.29	2.6 ± 0.8	0.06	11.23	11.90	346
NGC 6338	$2.13^{+0.19}_{-0.07}$	0.44 ± 0.01	3.7 ± 1.0	9.4 ± 0.3	22.6 ± 10.2	0.55	34.6 ± 14.7	0.05	11.54	12.37	651
NGC 7619	$1.06^{+0.07}_{-0.03}$	0.44 ± 0.01	7.9 ± 0.5	1.5 ± 0.1	3.2 ± 0.7	0.45	3.2 ± 1.2	0.12	11.44	12.12	557

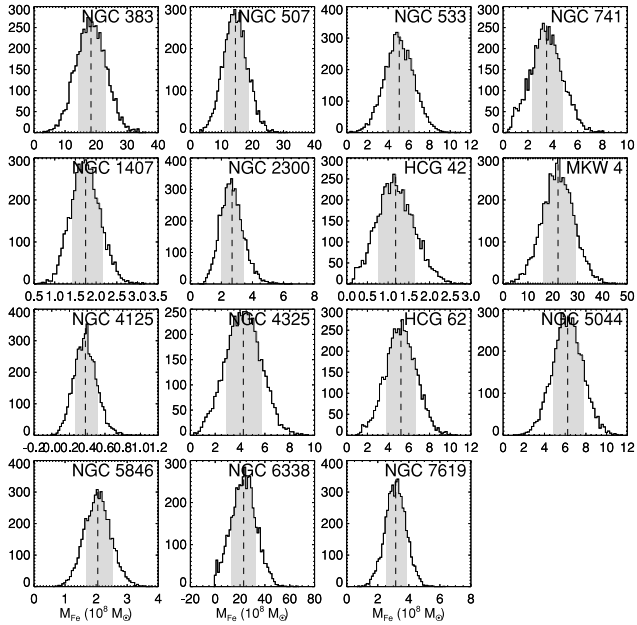

Figure 2. Illustration of the Monte Carlo output for the calculation of gas and metal masses and their uncertainties. Histograms show the obtained distribution of Fe masses for each group, with the resulting mean values represented by dashed lines, and the associated $\pm 1\sigma$ uncertainty ranges by the shaded area.

and abundances ($Z_{\rm Fe}, Z_{\rm Si}$) in each radial bin were drawn from Gaussians with σ equal to the associated 1σ error. The final metal mass and its uncertainty were then obtained as the mean and σ of the resulting distribution of masses. These distributions are generally symmetric, as illustrated in Fig. 2 which shows an example outcome of this approach for the calculation of Fe masses.

As is the case for the abundance profiles, the gas density profiles have generally not been measured out to r_{500} within our sample. Where relevant, the adopted β-parameters were therefore used to extrapolate the gas density profile of each group beyond the radius of measurement. Systematic uncertainties related to this extrapolation are not straightforward to quantify, because the number of gas mass measurements extending to r_{500} in $T \lesssim 2$ keV systems are still fairly limited (see e.g. Sun et al. 2009). *XMM–Newton* studies of groups to large radii (Rasmussen & Ponman 2004) suggest that standard β-models can provide a good description of the profiles of relaxed groups out to, and beyond, r_{500}. However, several studies have found the slope of the gas density profile in more massive clusters to steepen progressively at large radii, with typical slopes at r_{500} that are $\sim$15 per cent steeper than the 'canonical' cluster value of $\beta \approx 2/3$ (e.g. Vikhlinin et al. 2006; Maughan et al. 2008). To account for this steepening, Vikhlinin et al. (2006; see also Sun et al. 2009) multiply the standard β-model for the density profile by a factor $[(1 + r^\gamma/r_{\rm s}^\gamma)^{\epsilon/\gamma}]^{-1}$, with $\gamma = 3$ and $r_{\rm s}$ and ϵ fitted parameters.

Although the Vikhlinin et al. (2006) study was largely limited to $\langle T \rangle \gtrsim 2$ keV systems (leaving it unclear to what extent these results can be reliably extended to the regime of cool groups, whose density profiles inside r_{500} tend to be flatter than those of clusters; Sanderson et al. 2003), we have investigated the impact of adopting the Vikhlinin et al. (2006) parametrization for our groups. Mean values for the Vikhlinin clusters are $r_{\rm s} = 1.1 r_{500}$ and $\epsilon = 3.2$ (from their table 2), with no systematic dependence of these parameters on cluster temperature; adopting these values, we find that our gas masses within r_{500} could, on average, be overestimated by 24 per cent (with a small standard deviation of 4 per cent). This is within the adopted systematic uncertainty on $M_{\rm gas}$ (see Section 2.4), so within these adopted errors, our gas masses should be robust towards such changes in the assumed shape of the density profile. Furthermore, any trends in $M_{\rm gas}$-based quantities with mean system temperature would not be significantly affected by such a change. Many of the cluster comparison results presented in the following may also be subject to similar corrections, so our overall conclusions should remain valid irrespective of such a change.

2.3 Optical, near-infrared and radio properties

In order to derive mass-to-light ratios and to estimate the expected supernova rate in the groups, K- and B-band luminosities of the group members were also derived inside r_{500}. Luminosities were computed from extinction-corrected galaxy magnitudes in NASA/IPAC Extragalactic Database (NED) using the method of Osmond & Ponman (2004): Galaxies were extracted inside r_{500} and within a velocity interval of $3\sigma_v$ around the mean recession velocity $v_{\rm r}$ of the group, using starting values of $v_{\rm r}$ and velocity dispersion $\sigma_{\rm v}$ from Osmond & Ponman (2004) where available, or from Mulchaey et al. (2003) otherwise. These quantities were then re-evaluated iteratively until convergence was reached. The only exception to this rule was NGC 1407, for which a velocity range extending to $3.6\sigma_{\rm v}$ was employed. This was done in order to include the second BGG, NGC 1400, which has an unusually large peculiar velocity of $\sim$1100 km s^{-1} relative to the group mean (Trentham, Tully & Mahdavi 2006).

The adopted K-band magnitudes of the group members generally derive from Two-Micron All Sky Survey (2MASS) data (Skrutskie et al. 2006). Inspection of a composite histogram of the apparent magnitudes suggests that incompleteness sets in around $m_{\rm K} \approx 12.5$ for our groups, consistent with the expectation that the 2MASS source catalogue is 90 per cent complete down to $m_{\rm K} = 13.5$ for extended sources more than 30° from the Galactic plane (Skrutskie et al. 2006), a region covering 12 of our 15 groups. For each group, we corrected for incompleteness below the absolute magnitude corresponding to $m_{\rm K} = 12.5$ using the Schechter fit of Lin, Mohr & Stanford (2004) to the K-band luminosity function of 93 groups and clusters (and including their correction factor to obtain the Schechter normalization inside r_{500} instead of r_{200}). The resulting corrections are typically small, on average 5 per cent.

In order to facilitate comparison to existing results in the literature, B-band magnitudes of the group members were also extracted from NED in a similar manner. In four of the groups, magnitudes had to be converted from the R band for a few galaxies. This was done assuming $B - R = 1.5$ as is appropriate for early-type galaxies. While this could lead to a slight underestimation of L_B, we found that using instead $B - R = 0.8$ as for spirals resulted in a mere 4 per cent increase in L_B for NGC 4325, with the change being less than 0.5 per cent for the remaining three groups. We have refrained from taking these minute corrections into account in the error budget. Since the optical magnitudes generally derive from a variety of heterogeneous data sets with varying completeness, we have not attempted a similar correction for incompleteness as applied to the K-band data. Following Osmond & Ponman (2004), we instead simply aimed to homogenize completeness across the sample by applying an absolute magnitude cut to all groups. This cut discarded galaxies fainter than $M_B = -16.32$, retaining an expected 90 per cent of the B-band luminosity of the galaxy population.

Finally, using the derived B- and K-band luminosities and the corresponding $B-K$ colours, estimates of the total stellar masses M_* of the groups and their central galaxies were obtained using the coefficients listed in table 1 of Bell & de Jong (2001), which imply

$$\log\left(\frac{M_*/L_K}{M_\odot/L_\odot}\right) = 0.212(B-K) - 0.959 \quad (2)$$

for the K-band stellar mass-to-light ratio of the group members. We note that our approach implies that our $B-K$ colours could be slightly but systematically biased towards the red, because we are attempting to account for all K-band light by performing a completeness correction while only retaining an expected 90 per cent of the B-band light. This could lead to overestimates of stellar mass which, while potentially varying from group to group, should not exceed 0.02 dex, i.e. 5 per cent, and so this bias has no substantive impact on our results.

2.4 Robustness of results

Although not themselves the focus of this study, reliable gas masses are still important ingredients in this work, so we briefly discuss the robustness of our adopted approach. For example, while the derived statistical errors from our Monte Carlo calculations are small for most groups, one concern is whether the adopted β-parameters and our method of normalizing the density profile are robust. Another is that our approach does not take into account radial variations of the plasma emissivity. To explore the potential impact of this, we have compared our gas mass estimates to published values for the groups for which we have been able to find useful comparison data in the literature, consisting of either *Chandra*, *XMM* or *Suzaku* measurements published within a given radius using different approaches (Morita et al. 2006; Gastaldello et al. 2007; Komiyama et al. 2009). At larger radii, we have also compared our results within r_{500} to those obtained using the density parametrizations of Sanderson & Ponman (2003) based on *ROSAT* data. This comparison is shown in Fig. 3.

The figure indicates that there is no clear systematic variation between our results and other estimates, with most estimates agreeing to within ∼25 per cent. An exception is the clearly discrepant NGC 5846, for which the Sanderson & Ponman (2003) parametrization yields a gas mass within r_{500} which is only 65 per cent of our estimate. However, even when including this system, the average deviation of our estimates from existing results is only 10 per cent for all measurements, or 17 per cent if only including the independent largest radius estimate for each group. We therefore consider a 25 per cent error a reasonably conservative estimate of the systematic uncertainty associated with our method of gas mass estimation, so we have added this uncertainty in quadrature to those related to any quantity based on $M_{\rm gas}$.

Since the time of our original *Chandra* analysis, performed using CIAO 3.0 with calibration data base CALDB 3.2.3, updated calibration data including a recalibration of the *Chandra* effective area have been released. To briefly test the potential impact of this update on our results, we rederived the temperature and abundance profiles for NGC 4325, a group typical of our sample in terms of signal-to-noise ratio and mean ICM temperature. For this updated analysis, we employed the most recent calibration data, CALDB 4.1.2, with CIAO 4.1, following the spectral fitting procedure described in Paper I. We find that the updated temperature measurements are perfectly consistent with the original values in all radial bins, and the results for the Fe and Si profiles, shown in Fig. 4, also demonstrate good consistency throughout, with no systematic offset between the new and original results. In fact, the main effect of using the updated calibration data is a considerable reduction in the statistical uncertainties of most measurements. We therefore conclude that our original results should generally be robust to the recent changes to the *Chandra* calibration.

As a further indicator of the robustness of our abundance measurements, we point to the good overall agreement with the independently obtained *XMM* results presented by Finoguenov et al.

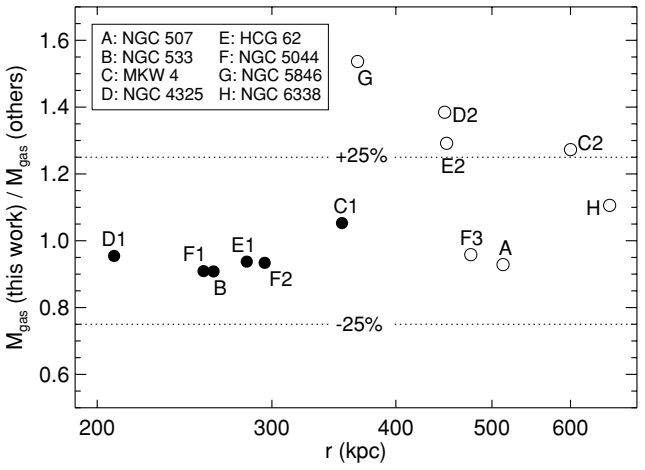

Figure 3. Ratio of our estimated gas masses to other published results. Filled symbols are based on measured values from the literature, empty ones on our values within r_{500} (Table 1) compared to those resulting from extrapolating the gas density parametrizations of Sanderson & Ponman (2003) to the same physical radius. Dotted lines mark a 25 per cent difference from equality. Comparison values for $M_{\rm gas}$ are *B*: $8.7 \times 10^{11}\,M_\odot$ within $r = 262$ kpc (Gastaldello et al. 2007); *C1*: $2.8 \times 10^{12}\,M_\odot$ (Gastaldello et al. 2007, $r \leq 353$ kpc); *D1*: $6.6 \times 10^{11}\,M_\odot$ (Gastaldello et al. 2007, $r \leq 208$ kpc); *E1*: $1.6 \times 10^{12}\,M_\odot$ (Morita et al. 2006, $r \leq 283$ kpc); *F1*: $9.9 \times 10^{11}\,M_\odot$ (Komiyama et al. 2009, $r \leq 256$ kpc); *F2*: $1.2 \times 10^{12}\,M_\odot$ (Gastaldello et al. 2007, $r \leq 295$ kpc).

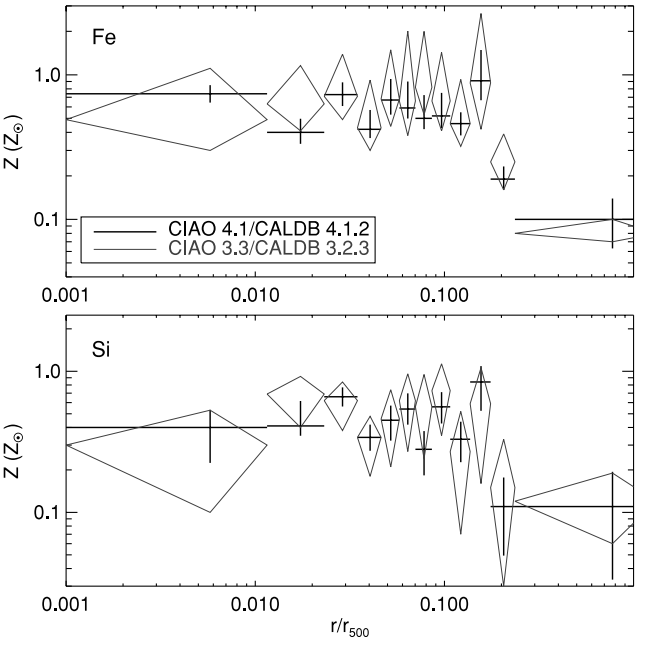

Figure 4. Comparison of (top) Fe and (bottom) Si profiles derived for NGC 4325 using the most recent *Chandra* calibration data (black crosses) and those of our original analysis in Paper I (grey diamonds).

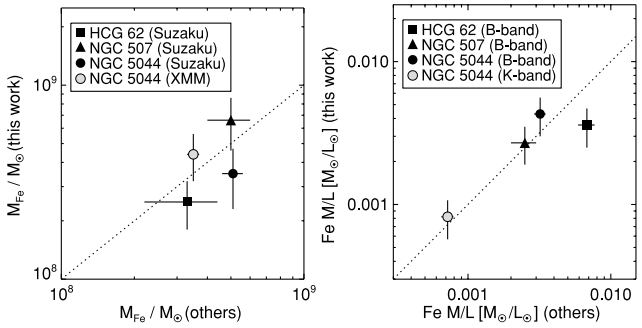

Figure 5. Comparison of (left) our Fe masses and (right) mass-to-light ratios to existing results, where available. Dotted lines represent equality.

(2006, 2007) (see discussion in Paper I), in particular the excellent agreement across the full radial range between our sample-averaged Fe profile in Fig. 1 and the corresponding *XMM* result (Johnson et al., in preparation). Encouragingly, good agreement is also seen when comparing our metal masses derived within specific radii to the corresponding *XMM* results for NGC 5044 (Buote, Brighenti & Mathews 2004) and the *Suzaku* results for HCG 62 (Tokoi et al. 2008), NGC 507 (Sato et al. 2009) and NGC 5044 (Komiyama et al. 2009), once differences in the adopted abundance table have been taken into account. This is illustrated in Fig. 5 (left-hand panel), demonstrating consistency at the $\sim 1\sigma$ level between ours and existing results in all four cases. Comparing also our resulting Fe mass-to-light ratios to the corresponding *Suzaku* estimates in Fig. 5 (right-hand panel), good overall agreement is again seen, with HCG 62 as the only exception. Since the derived Fe masses for this group are consistent, this discrepancy stems from differences in the assumed value of L_B within $r = 13$ arcmin, with the value of Tokoi et al. (2008), $L_B = 4.9 \times 10^{10}\,\mathrm{L}_\odot$ (derived by converting *R*-band magnitudes to the *B*-band magnitudes assuming a fixed *B*–*R* colour), being significantly lower than our value of $L_B = 7.6 \times 10^{10}\,\mathrm{L}_\odot$ obtained with the approach outlined in the previous section. This minor issue notwithstanding, we conclude that our results for both gas masses, metal masses and metal mass-to-light ratios generally show good agreement with existing results in the literature, thus lending credibility to our approach.

3 RESULTS

This section summarizes the derived group properties that will form the basis of the discussion in the following sections. Table 1 lists the main group properties used in this study, including the mean temperature $\langle T \rangle$ of each group derived inside the range $0.1 - 0.3 r_{500}$ (from Paper I), the adopted gas density parameters, derived metal masses inside r_{500} and their fractional contribution from SN Ia, the total *B*- and *K*-band luminosities inside the same radius and the derived galaxy velocity dispersions. Some of the properties of the BGG in each system (in all cases an early-type galaxy at the centre of the X-ray emission) are also relevant to the following discussion. In addition to stellar masses derived using equation (2), we have also compiled central stellar velocity dispersions $\sigma_{0,*}$ for these galaxies from Hyperleda (available for all the BGGs except NGC 4325 and 6338), and the 1.4-GHz luminosity density of any central radio source, based on fluxes listed in NED. These results are listed in Table 2.

Based on the parametrized Si/Fe ratios in Fig. 1 and the adopted SN yields, the abundance profiles have been decomposed into sample-averaged contributions from the two SN types in Fig. 6.

Table 2. Summary of relevant properties of the brightest group galaxy, including the derived stellar mass, central stellar velocity dispersion and 1.4-GHz radio power of any central radio source.

BGG	L_K ($\log \mathrm{L}_\odot$)	M_* ($\log \mathrm{M}_\odot$)	$\sigma_{0,*}$ (km s^{-1})	$P_{1.4}$ (W Hz^{-1})
NGC 383	11.66	11.69	278	3.4×10^{24}
NGC 507	11.69	11.55	308	3.7×10^{22}
NGC 533	11.72	11.56	273	2.2×10^{22}
NGC 741	11.81	11.65	295	7.2×10^{23}
NGC 1407	11.48	11.37	273	6.8×10^{21}
NGC 2300	11.24	11.15	261	4.8×10^{20}
HCG 42	11.71	11.57	320	...
MKW 4	11.90	11.77	275	1.9×10^{22}
NGC 4125	11.27	11.12	227	1.7×10^{21}
NGC 4325	11.35	11.26	...	...
HCG 62	11.62	11.65	232	1.6×10^{21}
NGC 5044	11.33	11.13	237	5.0×10^{21}
NGC 5846	11.51	11.39	237	2.3×10^{21}
NGC 6338	11.78	11.67	...	1.1×10^{23}
NGC 7619	11.55	11.42	322	7.3×10^{21}

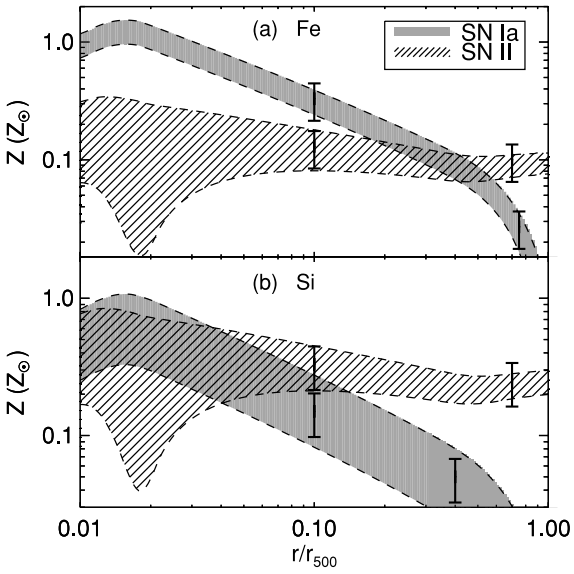

Figure 6. Sample-averaged contributions to the total abundance of (a) Fe and (b) Si from SN Ia and SN II, based on our $Z(r)$ parametrizations. Error bars at $0.1 r_{500}$ and at large radii show the adopted characteristic uncertainties of 35 per cent.

Errors in this diagram were propagated from the adopted statistical errors on our parametrizations of $Z_{\mathrm{Fe}}(r)$ and $Z_{\mathrm{Si}}(r)$, but are dominated at most radii by those related to the SN yields. The latter were evaluated by varying the assumed SN yields according to the different SN Ia and SN II models tabulated by Iwamoto et al. (1999) and Gibson, Loewenstein & Mushotzky (1997), respectively, subject to the constraint $Z_{\mathrm{Si}}/Z_{\mathrm{Fe}} > 2.0$ for SN II, as required by our results at large radii in Fig. 1. At each radius, the resulting maximum deviation relative to the case of our 'reference' yields was taken as the uncertainty associated with the assumed SN yields and then added in quadrature to the statistical errors on the abundance parametrizations. The shaded regions in Fig. 6 outline the resulting lower and upper limits. The large uncertainties for Si in particular derive mainly from the significant variations in predicted SN Ia Si yields (0.14–0.27 $\mathrm{M}_\odot$) among the models considered. Nevertheless, at most radii $r \gtrsim 0.1 r_{500}$ considered in this study, the

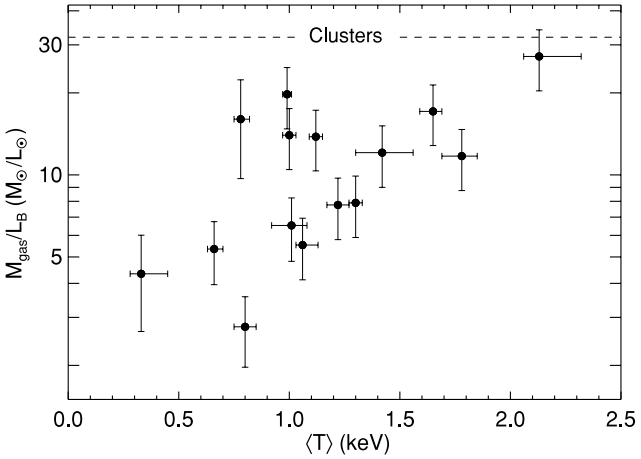

Figure 7. Gas mass-to-light ratio inside r_{500}. Dashed line shows the mean value of the $T > 4$ keV clusters of Finoguenov et al. (2003).

resulting uncertainties can be accounted for by assuming a characteristic error of 35 per cent, illustrated by the fiducial error bars in Fig. 6. Wherever relevant, we have taken this uncertainty into account in the error budget by adding it in quadrature to existing errors, for example when computing total metal masses contributed by either SN type. We also stress that while Fig. 6 remains useful as a representation of the sample-averaged results, the SN decomposition for individual groups was performed using the actual measurements pertaining to each group, with the results in the figure being employed only when extrapolation to r_{500} was necessary.

In accordance with results for clusters, Fig. 6 establishes on a firmer basis the results of Finoguenov et al. (2000) that SN Ia products in groups are centrally concentrated, contributing about 80 per cent of the Fe in group cores, and that SN II products on average are more uniformly distributed, showing only mildly increased central levels. Fe produced by SN II therefore dominates at large radii both in groups and in clusters. Fe enrichment levels in the central metal excesses are comparable to those in cool-core clusters and are clearly dominated by SN Ia as also found in clusters (De Grandi et al. 2004; de Plaa et al. 2007), but cannot be entirely explained by a central excess in SN Ia products alone unless assuming non-standard SN Ia yields. This agrees with the earlier result of Finoguenov & Ponman (1999) based on a sample of only three groups, as does the derived SN II contribution to the Fe abundance at large radii of 0.05–0.1 $Z_\odot$.

Total gas masses normalized by optical luminosity are summarized in Fig. 7. The figure reveals large variations in the ratio of gas mass to *B*-band light, and suggests a systematic dependence on $\langle T\rangle$, albeit one subject to significant scatter (Kendall's $\tau = 0.35$, correlation significance $\sigma_K = +1.8$, which reduces to $\sigma_K = 1.6$ if using L_K instead of L_B). Inferred values range from 3 to 30 $M_\odot/L_\odot$, with a mean of $12 \pm 2\,M_\odot/L_\odot$ for groups in the $T = 1$–2.2 keV range. Although the latter value is in good agreement with results of cosmological simulations (Romeo et al. 2006), it is nominally somewhat lower than the corresponding value of $\approx 20\,M_\odot/L_\odot$ found by Finoguenov, Burkert & Böhringer (2003), and the overall implication of Fig. 7 is that gas mass-to-light ratios in our groups are well below typical cluster values.

3.1 Metal masses and mass-to-light ratios

The results for the total X-ray metal masses in the groups are summarized in Fig. 8, including the decomposition into contributions from SN Ia and SN II. Also shown are the corresponding metal mass-to-light ratios, all presented as a function of mean group temperature $\langle T\rangle$. We note that $\langle T\rangle$ correlates with total L_B, L_K, M_*, and velocity dispersion σ_v at 3.6–3.8σ significance, suggesting that none of these parameters is a seriously biased proxy for total group mass. Also note that we generally normalize by L_B rather than L_K or stellar mass in these plots in order to enable straightforward comparison to existing results in the literature. Since total L_K and L_B are tightly correlated for the sample ($\sigma_K = 4.9$), this particular choice should have little bearing on the qualitative trends or the degree of intrinsic scatter seen in the figures.

As can be seen from Table 1 and Fig. 8, the total Fe and Si masses derived inside r_{500} span two orders of magnitude across the sample, roughly from $M \sim 3 \times 10^7$– $3 \times 10^9\,M_\odot$ for both elements, and with a clear dependence on total group 'mass' $\langle T\rangle$ as anticipated. For Si, the higher abundance observed at large radii (cf. Fig. 1) roughly compensates for its lower atomic mass relative to Fe, yielding rather similar aggregate masses for the two elements in most cases. The fractional contribution by SN Ia to the metal production as listed in Table 1 implies that, on average, SN II have generated ∼60 per cent of the Fe and ∼90 per cent of the Si inside r_{500}. There is a weak tendency for these fractions to decrease with $\langle T\rangle$, $\sigma_K = -1.6$ ($\sigma_K = -2.1$ if excluding the clearly discrepant NGC 4325), suggesting that enrichment in cooler systems is slightly more SN II-dominated.

The iron mass-to-light ratio (IMLR) represents a key quantity for studies of enrichment in groups and clusters, as it is expected to reflect the ability of a system to generate and retain enriched material within its gravitational potential. As already mentioned, the derived Fe abundances of our groups at large radii, where most of the gas resides, are lower than the corresponding cluster values by a factor of ∼2. As discussed in Paper I, a similar deficit, if slightly smaller, is also observed for Si. The combination of a lower metal content in the hot gas and generally lower gas mass-to-light ratios in groups compared to more massive clusters (cf. Fig. 7; see also Lin, Mohr & Stanford 2003) should manifest itself in lower total metal *M*/*L* ratios in cool systems. For iron, we note that a similar conclusion was already put forward by Renzini (1997) on the basis of *ROSAT* and *ASCA* data collected from the literature. However, this study used global abundance measurements out to the radius of X-ray detection, thus neglecting the important fact that X-ray emission in groups is generally detected to relatively smaller radii than clusters. Since cumulative M_{Fe}/L_B ratios tend to rise outwards because the gas generally has a flatter distribution than that of the optical light (e.g. Finoguenov et al. 2000; Sato et al. 2009), the bias thus introduced will result in lower values in X-ray faint systems, even if the intrinsic Fe *M*/*L* ratio inside a fixed fraction of the virial radius did not vary between groups and clusters. The problem is only aggravated by the fact that groups typically have shallower gas distributions than clusters and so contain a relatively larger fraction of their hot gas (and metals) at large radii. A fair comparison between systems of differing X-ray brightness therefore requires all systems to be consistently compared within a fixed overdensity radius.

These issues prompted us to investigate aggregate metal mass-to-light ratios of our groups for comparison to clusters. The results within r_{500} are also shown in Fig. 8. The inferred ratios vary by a factor of ∼10 across the sample, with indications of both M_{Fe}/L ($\sigma_K = 2.1$) and M_{Si}/L ($\sigma_K = 2.3$) systematically increasing with group temperature. Note that this is despite the fact that our temperature-independent $Z(r)$ parametrizations, adopted for the groups for which the abundance measurements do not extend to

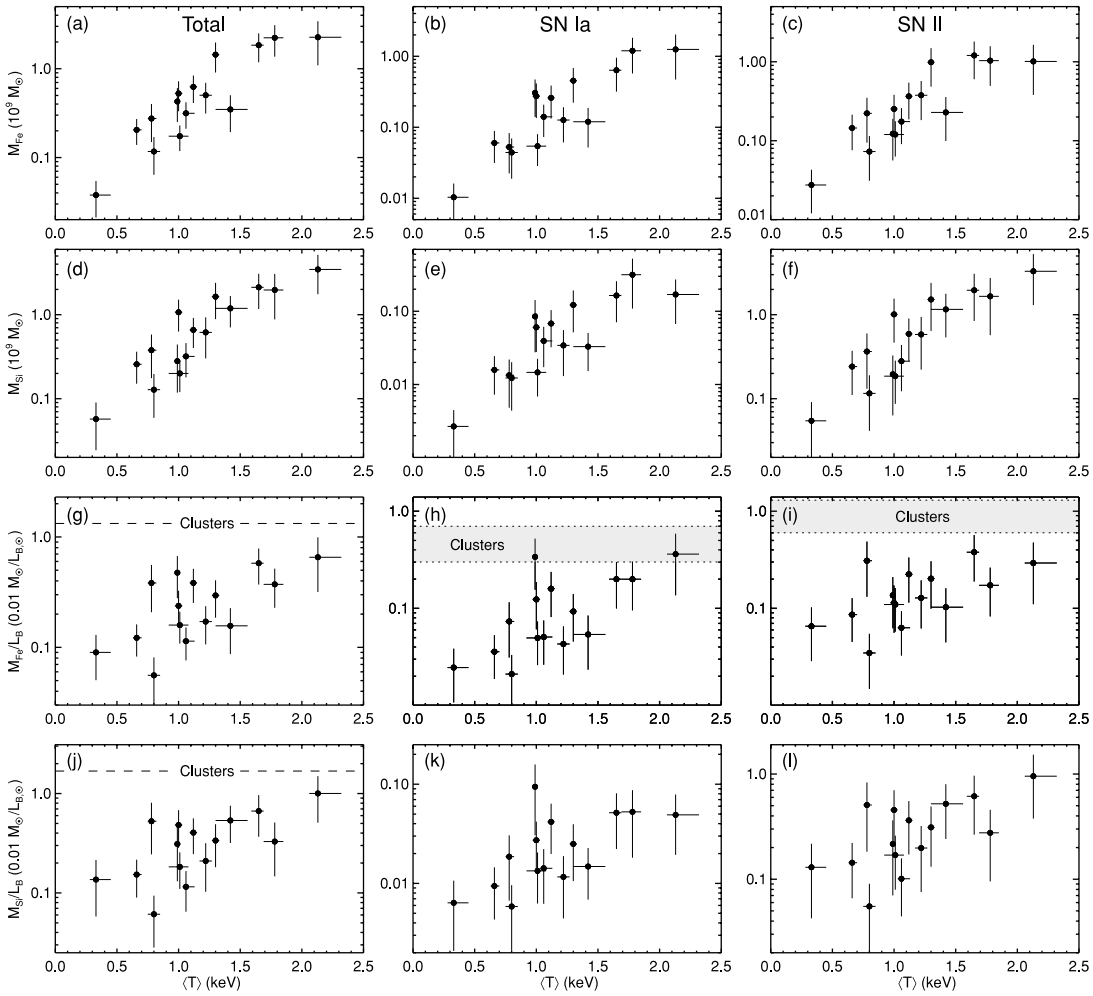

Figure 8. Left-hand panel: derived total masses of Fe and Si inside r_{500} as a function of mean group temperature $\langle T \rangle$, along with the corresponding B-band mass-to-light ratios. Centre and right-hand panels show the results decomposed into contributions from SN Ia and SN II, respectively. Dashed lines show the mean values for the $T > 4$ keV clusters of Finoguenov et al. (2003), and shaded regions mark the typical cluster ranges from Finoguenov et al. (2000).

r_{500}, will tend to suppress trends with $\langle T \rangle$ (the main motivation for showing Fig. 8 in its current form is to facilitate comparison to more massive systems, for which results are typically provided within r_{500}). The results clearly suggest lower Fe (and Si) mass-to-light ratios in cooler systems, with both ratios only approaching typical cluster values at the high-T end covered by our sample. We note that this apparent shortfall of metals in groups is not simply an artefact of our choice of cluster comparison data. For example, the $T > 3$ keV clusters of De Grandi et al. (2004) display an IMLR within r_{500} of $1.7 \pm 0.3 \times 10^{-2}$ for our adopted value of H_0, even higher than the $\approx 1.3 \times 10^{-2}$ reported by Finoguenov et al. (2003). Using a considerably larger group sample than that of Finoguenov et al. (2000), we thus confirm their tentative result that groups generally have Fe M/L of $\lesssim 0.006$ at all radii $r \lesssim r_{500}$ and tend to show lower $M_{\rm Fe}/L_B$ than clusters at a fixed overdensity radius.

In order to infer the origin of the lower metal mass-to-light ratios in cool systems, a key question to address is whether the shortfall of Fe compared to clusters is present both for SN Ia and for SN II products. In Figs 8(h) and (i), the IMLR has been decomposed into contributions from SN Ia and SN II (denoted by $\rm IMLR_{Ia}$ and $\rm IMLR_{II}$ in the following). This clearly reveals a deficit of Fe from *both* SN types in groups, a conclusion also reached by Finoguenov & Ponman (1999), possibly suggesting a combination of responsible mechanisms. We note that Finoguenov & Ponman (1999) and Finoguenov et al. (2001) see a clear increase in $\rm IMLR_{II}$ with T for clusters ($T > 2$ keV), and a global deficit of SN II ejecta in groups (as do we), but their cluster $\rm IMLR_{Ia}$ is nearly constant with T across the full range covered by their systems, at variance with our results in the group regime.

3.2 Dependence on ICM temperature

Figs 7 and 8 suggest that the observed variation in IMLR among the groups is driven primarily by a systematically increasing gas mass-to-light ratio with mean group temperature. In order to also investigate any temperature dependence on abundance structure, the binned abundance profiles of Fig. 1 were split into results for 'cool' ($T \leq 1.1$ keV) and 'warm' ($T > 1.1$ keV) groups in Fig. 9. We repeat here that $\langle T \rangle$ was derived within the fixed radial range $0.1-0.3r_{500}$, and so is not affected by the strong central cooling seen in most of the groups (cf. Paper I). Evidently, Fe abundances in cooler groups tend to be lower at all radii common for the two subsamples. This conclusion is clearly robust inside $r \lesssim 0.5r_{500}$, as will be demonstrated quantitatively below, but the situation is less clear at larger radii where only a few of the 'cool' groups within our sample have useful *Chandra* data. The results for Si are

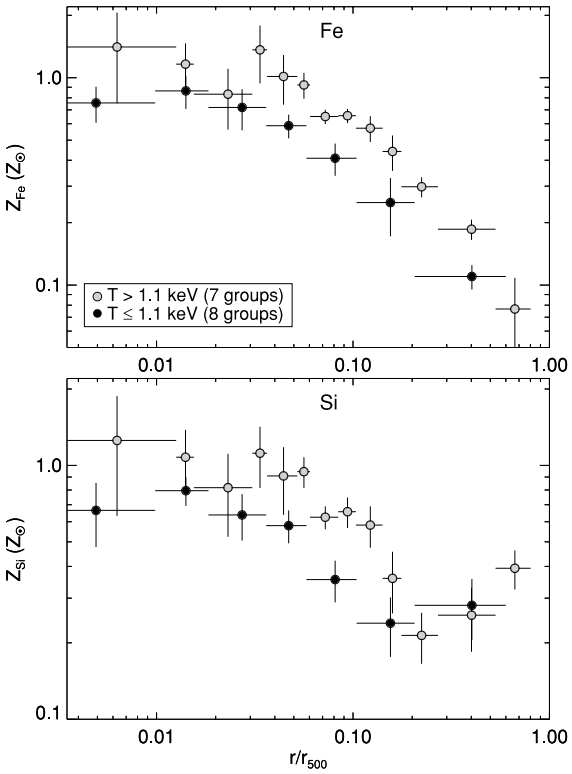

Figure 9. Stacked Fe and Si profiles for 'cool' ($\langle T\rangle \leq 1.1$ keV) and 'warm' ($\langle T\rangle > 1.1$ keV) subsamples separately, in radial bins of 10 data points.

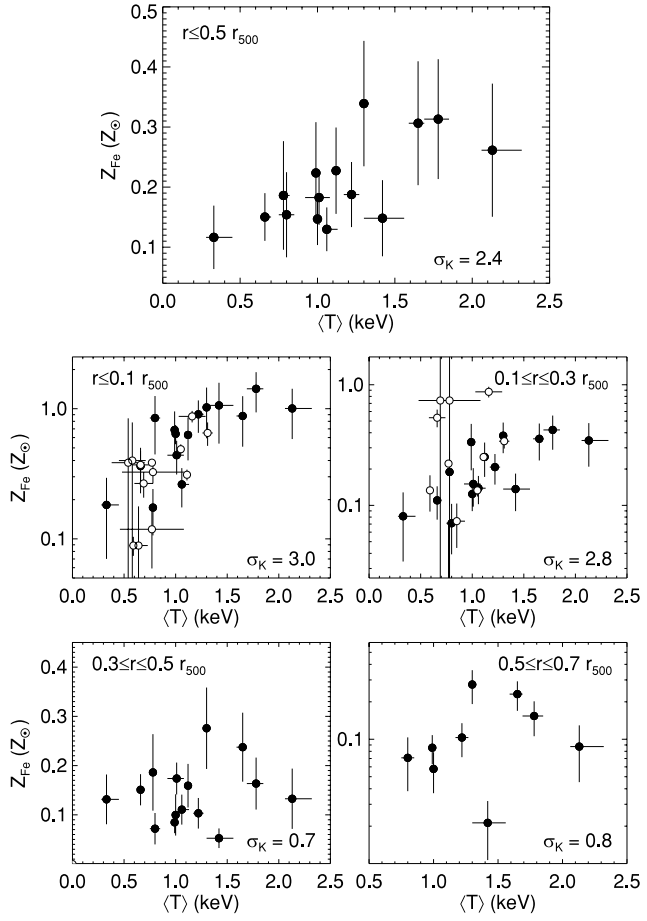

Figure 10. Mass-weighted Fe abundances within various radial ranges. Our results are marked with filled circles, with the results of Finoguenov et al. (2006, 2007) included as empty circles where relevant. Only groups with data covering the full radial interval are shown in each plot. Labels in lower right corners specify the significance σ_K of any linear correlation among our own data points.

qualitatively similar to those of Fe in the group cores ($r \lesssim 0.1$–$0.2r_{500}$), but at larger radii there are no obvious differences between the two subsamples. Note also that the poorer statistics resulting from dividing the sample masks the clear indication of a central abundance dip seen in Fig. 1.

Fig. 9 indicates a general trend of higher metal abundances in hotter groups, at least in their central regions. To explore this quantitatively while also accounting for any systematic differences in the amount and distribution of gas with system temperature, we consider in Fig. 10 the Fe mass-to-gas ratios, effectively the mass-weighted Fe abundances. The top panel shows the ratios within $0.5r_{500}$, for which we have measurements for all groups and do not have to rely upon the (temperature-independent) radial abundance parametrizations. Within this radius, there is evidence for a systematic increase in mean Z_{Fe} with $\langle T\rangle$ at a moderate significance level of 2.4σ. The following panels break this down into separate radial intervals, only including groups with data in the relevant range in each plot. For the relevant radial ranges, we have also included the 14 *XMM* groups of Finoguenov et al. (2006, 2007) that are not part of our sample and for which results have been extracted in a similar way. There is convincing evidence of an increasing Fe abundance with system temperature in the cores of these groups, but the trend progressively disappears as one moves to larger radii, and is significant at less than 1σ beyond $0.3r_{500}$. This conclusion is only strengthened by the inclusion of the Finoguenov et al. data points in the correlation analyses, with which σ_K rises to $+4.1$ within $0.1r_{500}$ and drops to $+2.1$ within $0.1 \leq r \leq 0.3r_{500}$. The overall picture for Si is very similar, with a clear positive correlation within $0.1r_{500}(\sigma_K = +2.5)$ but none further out. We emphasize that the absence of a clear trend at large radii supports our use of a single parametrization to describe the abundance profiles beyond the radius of X-ray detection where necessary. Outside the core, similar results have been reported by Tamura et al. (2004) for T and Z derived within the range 50–200 h^{-1} kpc in a combined sample of groups and clusters, and by Finoguenov et al. (2001) for Z_{Fe} of $T \sim 1$ keV systems derived at $0.2r_{180}$. However, at small radii the clear trend seen here differs from results for clusters; for example De Grandi et al. (2004) find no clear correlation between Z and T measured inside r_{2500} for their $T > 3$ keV systems.

The observed trend in the group cores could potentially by induced by systematics, as suggested by the work of Buote (2000a), a Z–T correlation could arise due to the Fe and Si biases, which are more pronounced at low T. However, for most groups, the results in the core are based on mass-weighting spectral results extracted within narrow radial ranges in which T does not vary much. In the few cases where it does, two-temperature models were employed in spectral fitting, as described in Paper I, suggesting that we have generally resolved any temperature structure that could be affecting the abundance determinations. Further, the same overall trends are seen for the emission-weighted abundances, using Z directly from spectra extracted across the relevant radial range (which in some cases require two-temperature models for a satisfactory fit). This argues against a systematic effect related to the modelling of the density profiles in the group cores. We therefore conclude that the inferred trends should be reasonably robust against such biases.

3.3 Supernova feedback

In the context of elucidating the nature and history of galactic feedback in the groups, the SN contribution to ICM energetics is an important quantity. Based on the adopted SN yields, we computed the energy $E_{\rm SN}$ released by the two SN types, assuming that energy has been released to the ICM in proportion to the metals at a level of 10^{51} erg per supernova. Under this simplifying assumption, the specific SN energy – i.e. the total energy normalized by the number of ICM particles – released within r_{500} is shown as a function of group temperature in Fig. 11. In a study of cool clusters out to $0.4r_{180}$, Finoguenov et al. (2001) found a clear increase in specific $E_{\rm SN}$ with T across the range $T = 1$–3 keV, with the trend flattening above $T \gtrsim 3$ at 1.2 keV particle^{-1} (shown as a dotted line in Fig. 11). Our results sample the low-T end better and reveal no significant trend within r_{500} ($\sigma_{\rm K} = +0.1$), although a positive trend of weak significance ($\sigma_{\rm K} \approx +1$) is found within $0.6r_{500} \approx 0.4r_{180}$. Mainly as a consequence of the factor of 2 lower abundances in outskirts, the sample mean of $E_{\rm SN}$ is correspondingly lower for our groups than found for the Finoguenov et al. (2001) clusters. Note that Fig. 11 also suggests that $E_{\rm SN}$ becomes comparable to the thermal energy $E_{\rm th} = (3/2)kT$ of the ICM particles below $T \sim 0.5$ keV. While this is in excellent agreement with results of cosmological simulations incorporating galactic outflows (Davé, Oppenheimer & Sivanandam 2008), our results are inconsistent with the specific $E_{\rm SN}$ declining with $\langle T \rangle$ as predicted by those simulations.

The total SN energy released in the groups spans the range 4×10^{59}–2×10^{61} erg. Although SN Ia contribute about ∼20 per cent of the $E_{\rm SN}$ within the group core, the vast majority (∼95 per cent) of the total energy released within r_{500} has been provided by SN II. We emphasize, however, that these numbers, as well as those shown in Fig. 11, simply represent the SN explosion energy *associated* with the metals in the ICM and not necessarily the energy *delivered* by SN to the hot gas. The two quantities would differ if, for example, the fraction of synthesized metals reaching the ICM is different from the corresponding value for the SN explosion energy. We will return to these issues in Section 4.2, noting for now that uncertainties on the inferred $E_{\rm SN}$ are not necessarily dominated by those associated with our gas mass estimates or the choice of SN model yields.

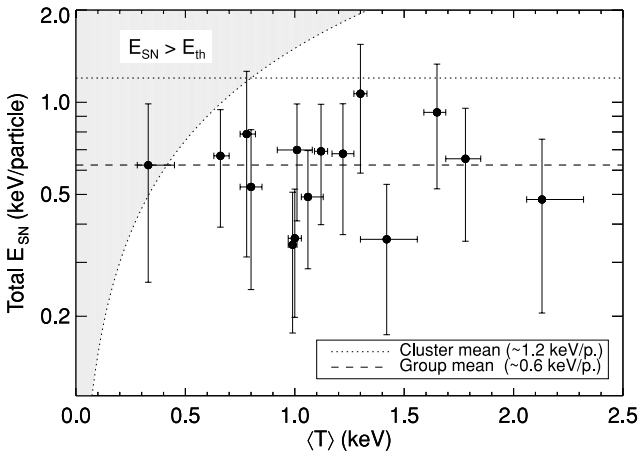

Figure 11. Released SN energy per ICM particle inside r_{500}. Dashed line marks our mean value of $E \approx 0.6$ keV particle^{-1}, while dotted line shows the mean found for $T \gtrsim 3$ keV clusters (Finoguenov et al. 2001). Shaded area shows the region where $E_{\rm SN}$ exceeds the thermal energy $E_{\rm th}$ of the ICM.

3.4 The origin of the central iron excess

The presence of a central Fe excess in these groups parallels results for clusters which show this feature to be common in cool-core systems (e.g. Finoguenov et al. 2000; De Grandi et al. 2004). As for clusters, the excess can extend well beyond the optical extent of the central galaxy and can show a dip at the very centre, inside $r \lesssim 0.5D_{25}$, where D_{25} is the ellipse outlining a B-band isophote of 25 mag arcsec^{-2}. As shown in Fig. 6, the enrichment in group cores has not been exclusively provided by SN Ia, but the Fe *excess* itself, relative to the Fe level at large radii, has largely been provided by SN Ia. This is broadly consistent with the idea that the central early-type galaxy is responsible for the Fe excess. While evidence for this conclusion is also observed in clusters (e.g. Böhringer et al. 2004; De Grandi et al. 2004), this scenario has not been tested in any detail in groups. One could a priori expect a similar situation to hold for lower mass systems, since the fractional contribution of the brightest galaxy to the total light is generally larger in these than in clusters (Lin & Mohr 2004).

In order to investigate this, we computed the mass of Fe produced by SN Ia within $0.1r_{500}$. On average, this corresponds to a radius of $r \approx 50$ kpc, roughly matches the radial extent of the cool core where present (cf. Paper I), and corresponds to twice the maximal D_{25} extent of the central galaxy and to the radius where the radially weakly declining SN II contribution to Fe production becomes consistent with the level in the outskirts (Fig. 6). Results were normalized by the K-band luminosity of the central galaxy from Table 2. Assuming our adopted SN Ia yields along with the observed present-day SN Ia rate in nearby early-type (E/S0) galaxies of $R_0 = 3.5^{+1.3}_{-1.1} \times 10^{-14}\,{\rm yr}^{-1}\,{\rm L}_{{\rm K},\odot}^{-1}$ (Mannucci et al. 2005), the resulting time-scales required for SN Ia in the central galaxy to generate the observed Fe mass are illustrated in Fig. 12(a). Results from Si broadly agree with those from Fe. As can be seen, there is a clear dependence of the Fe M/L ratio, and hence required enrichment time-scale, on $\langle T \rangle$ within $0.1r_{500}$, qualitatively mirroring the global behaviour inside r_{500} (cf. Fig. 8). Both the mean and median enrichment time-scales for the sample are ∼5 Gyr, which, given the increasing time-scale with T, is entirely consistent with the corresponding results of Böhringer et al. (2004), who find that times of $\gtrsim$5 Gyr are required in clusters.

The immediate implication is that in many of these groups, SN Ia in the central group galaxy could well be responsible for the Fe excess seen within the cool core. Some caveats to this interpretation, however, include the facts that our method does not include the Fe that has become locked in stars over the relevant time-scales [although this might be a small fraction if star formation (SF) largely ceased at high redshift in these central galaxies], nor do we account for any Fe expelled beyond 0.1 r_{500} by galactic winds, or for the growth of stellar mass ($\sim L_{\rm K}$) of the BGG over the considerable time-scales involved. The inferred time-scales may thus be viewed as lower limits under the adopted assumptions. On the other hand, there could be a contribution to central enrichment due to stellar mass loss in the BGG and due to gas lost to group cores from satellites via galactic winds or environmental interactions. A more sophisticated approach would thus include the contribution from stellar winds along with a model of the stellar mass evolution of the BGG. An argument for not considering the latter effect here, however, is the observation that the bulk of the stellar mass in many central cluster ellipticals was in place already at $z = 2$–3 (e.g. Stott et al. 2008), so this may not play an important role. A case specific to our sample is NGC 1407, in which the BGG appears to have formed over half its stellar mass already by $z \approx 5$ (Spolaor et al. 2008).

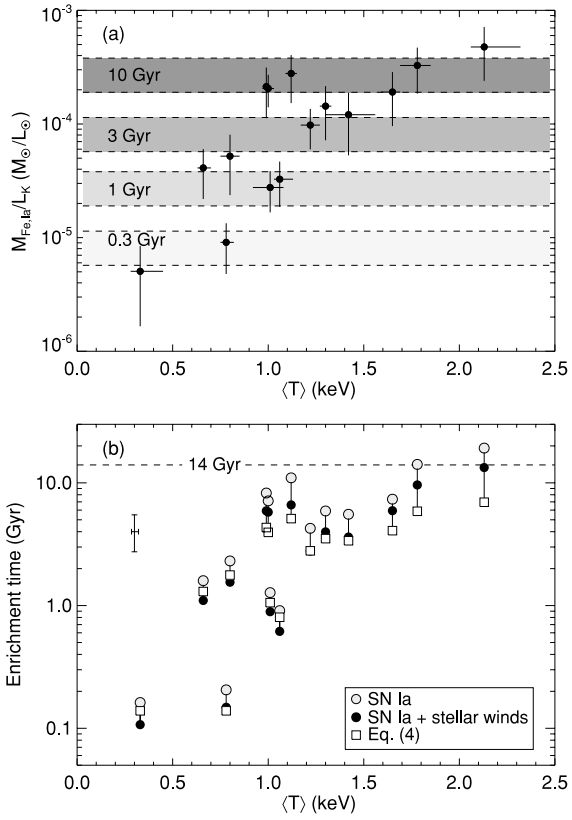

Figure 12. (a) Mass of Fe produced by SN Ia within $0.1r_{500}$, normalized to the K-band luminosity of the central group galaxy. Shaded regions outline the errors on the typical time-scales required for SN Ia to produce the observed $M_{\rm Fe}/L_{\rm K}$ ratios, assuming a constant SN Ia rate with redshift. (b) The corresponding enrichment times, including also the effect of stellar mass loss in the BGG, and that of assuming an SN Ia rate evolving with redshift according to equation (4). Lines connect the time-scales for each group as computed under these different assumptions. A typical error bar (dominated by uncertainties in the local SN Ia rate) is shown at $T = 0.3$ keV. Dashed line marks an enrichment time-scale of 14 Gyr.

Mass loss due to stellar winds can be trivially incorporated in our calculations, and it is instructive to consider the impact of this. For this purpose, we consider *all* the Fe present within $0.1r_{500}$ (i.e. not just that produced by SN Ia), but subtract a uniform base level of 0.1 $Z_\odot$ as seen in the group outskirts to obtain an estimate of the *excess* iron mass within this radius. Following Böhringer et al. (2004), the stellar mass loss rate $\dot{M}_*$ from the central early type is then estimated from

$$\frac{\dot{M}_*}{\mathrm{M}_\odot\ \mathrm{yr}^{-1}} \approx 1.5\times10^{-11}\frac{L_B}{\mathrm{L}_\odot}\left(\frac{t_*}{15\ \mathrm{Gyr}}\right)^{-1.3}, \qquad (3)$$

where t_* is the 'age' of the galaxy (Ciotti et al. 1991). The rate of Fe loss is obtained by multiplying this estimate by the mean Fe mass fraction in stellar winds, which in turn depends on stellar metallicity. Assuming mildly supersolar metallicities for the BGG stellar population ($Z = 1.5\,Z_\odot$, corresponding to [Z/H] $\approx +0.2$; see e.g. Sánchez-Blázquez et al. 2007) along with our adopted solar abundance table (Grevesse & Sauval 1998) and a typical galaxy age of 10 Gyr (Sánchez-Blázquez et al. 2006), the prediction of equation (3) is added to the SN Ia iron production rate and the associated enrichment times plotted in Fig. 12(b).

On average, the inferred stellar mass loss can account for ∼25 per cent of the Fe within $0.1r_{500}$, reducing the required enrichment times correspondingly. Nominally, this brings the estimated time-scales below 14 Gyr for all groups, alleviating – but not obviating – the need for additional sources of metal enrichment in the cores of high-T groups. Hence, subject to the adopted assumptions, the time-scales may still be prohibitively long for systems with high $M_{\rm Fe}/L_{\rm K}$ ratios in the core. Tentative evidence that satellite galaxies may have contributed to building up the central metal excesses in at least one of our groups is provided by Mendel et al. (2009), who demonstrate a good correspondence between the radial X-ray Fe distribution and that of stellar mass density in the NGC 5044 group out to $r \approx 100$ kpc, corresponding to five times the D_{25} extent of the BGG. Yet, barring a significant additional contribution to central Fe enrichment from other group galaxies, we are compelled to conclude that our approach generally underestimates the metal production of the BGG over cosmic time. Possible loopholes include invoking an SN Ia rate per unit $L_{\rm K}$ that evolves with redshift, similar to what has been proposed for early types in more massive clusters (e.g. Renzini et al. 1993; Böhringer et al. 2004), or a significant contribution to central ICM enrichment either from intracluster (IC) stars (see Section 4.2) or from the sinking of highly enriched low-entropy gas towards group cores (Cora 2006).

We can briefly explore the former possibility, the effect of a redshift-dependent SN Ia rate. To this end, we assume an evolving SN Ia rate $r_{\rm Ia}(t)$ per rest-frame time t and comoving volume as described by the star formation rate SFR(t) at a given time convolved with the SN Ia delay time distribution $\Phi(t)$,

$$r_{\rm Ia}(t) \propto \int_{t_0}^{t} \mathrm{SFR}(t')\Phi(t-t')\,\mathrm{d}t', \qquad (4)$$

where t_0 is the age of the Universe at the initial redshift of SF, here assumed to be at $z_{\rm f} = 10$. Following Ettori (2005), SFR(t) is adopted from the extinction-corrected model of Strolger et al. (2004), and Φ is assumed to be a Gaussian of characteristic delay time $\tau = 4$ Gyr and $\sigma = 0.2\tau$ (the results are not highly sensitive to the exact choice of Φ; see Ettori 2005). In this model, the SN Ia rate peaks at $z \approx 0.8$ at ≈4.8 times the present-day value. Excluding here the effects of stellar winds (for straightforward comparison to the results assuming a constant SN Ia rate with no stellar wind contribution), the resulting enrichment time-scales are plotted as empty squares in Fig. 12(b). This modification is seen to reduce the enrichment time-scales to ∼5–7 Gyr even for the hottest groups, in agreement with similar estimates for cluster BCGs (Böhringer et al. 2004). Thus, in this model, the central Fe excess can easily have been generated by the BGG itself within half a Hubble time, without the need for additional sources of central enrichment.

A final point worth mentioning here, related to mass loss through stellar winds, involves the associated abundance ratios. Since neither Si nor Fe is processed in the intermediate-mass stars primarily responsible for such winds, the α/Fe ratio of these winds (and of their parent stars) will be identical to that of the gas from which the stars formed. This ratio can generally be expected to be high in early-type galaxies, where SF was largely terminated at high redshift as indicated by the supersolar α/Fe ratios typically found for the stellar population in these galaxies (e.g. Sánchez-Blázquez et al. 2007). Consequently, stellar winds from our BGGs should have α/Fe ratios approaching those of SN II ejecta. Interestingly, Fig. 6 indicates a mild central enhancement in SN II abundances which is at least consistent with a significant contribution from stellar mass loss associated with the BGG. Whether this feature can be entirely explained by stellar mass loss is a complicated question, however. A contribution from SN II to central enrichment is certainly still required, as the predicted sample mean of $Z_{\rm Si}/Z_{\rm Fe} \approx 0.95$ from

SN Ia and stellar winds alone falls short of the observed mass-weighted mean of $Z_{\rm Si}/Z_{\rm Fe} \approx 1.10$ inside $0.1r_{500}$. The radial extent of the SN II enhancement suggests either a contribution from stars not currently in the BGG, i.e. other group members or IC stars, or the action of some gas and metal mixing within $\sim 0.3r_{500}$. Moreover, the spatial distribution of stellar mass loss products is not straightforward to predict, since both [Z/H] and [α/Fe] in early-type stellar populations tend to show radial gradients; while [Z/H] generally peaks towards the galactic centre, α/Fe gradients may be positive, negative, or flat, and the mean absolute value may depend on galaxy mass (Sánchez-Blázquez et al. 2007; Spolaor et al. 2009), implying that the Fe fraction and abundance ratio in stellar winds may be a highly non-trivial function of radius and of the environment of the BGG. A detailed exploration of this would likely require X-ray data of a superior quality and is beyond the scope of this study.

4 ORIGIN AND FATE OF ICM METALS IN GROUPS

We can briefly summarize the results of the previous section as follows. Cool-core groups tend to show similar levels of central enrichment to those of more massive systems, but abundance gradients outside the core are stronger, leading to lower abundances at large radii. Group outskirts are heavily dominated by SN II enrichment, with the total energy per ICM baryon injected by SN somewhat lower than in more massive systems. At the same time, the global gas mass for a given amount of stellar light is lower in cooler systems within r_{500}, leading to lower global metal mass-to-light ratios, for both SN Ia and SN II products. The latter result in particular may hold important information on the enrichment history of these systems. In this section, we investigate a range of possible explanations for this while acknowledging that this is not necessarily an exhaustive list. Fundamentally, these explanations can be divided into mechanisms causing (i) less efficient metal generation or metal transfer to the ICM in low-mass systems, (ii) removal of metals from groups over cosmic time or (iii) cosmological accretion of less enriched gas in small systems.

4.1 Galaxy formation efficiency and SF history

As an example of a mechanism belonging to the first category mentioned above, we first consider the possibility of a reduced galaxy formation efficiency at low $\langle T \rangle$. Everything else being equal, this would lower the amount of Fe released per unit ICM mass, and although this cannot in itself explain the observed IMLR variations (unless the stellar initial mass function also varies with environment), it could help explain the globally lower metal abundances seen in cooler systems.

We can test this scenario on the basis of the gas mass-to-light ratio in Fig. 7, or equivalently, the ratio of stellar mass M_* to that of baryons, $M_{\rm bar} \approx M_* + M_{\rm ICM}$ (sometimes denoted the cold fraction $f_{\rm c}$, or the SF efficiency) shown in Fig. 13. This plot indicates a general decrease in cold fraction with $\langle T \rangle$ ($\sigma_{\rm K} = -1.5$, strengthening to $\sigma_{\rm K} = -2.2$ if excluding the somewhat peculiar NGC 2300; see Paper I), but with a tendency for this quantity to be higher than corresponding results for clusters (Ettori 2003). Hence, the galaxy formation efficiency actually appears to *rise* in lower mass systems within our sample, in concordance with other observational and theoretical findings (Lin et al. 2003; Romeo et al. 2006; Gonzalez, Zaritsky & Zabludoff 2007; Davé et al. 2008). Hence, there is no relative dearth of stellar mass within our groups, and we can readily exclude more exotic scenarios to account for the lower IMLR such

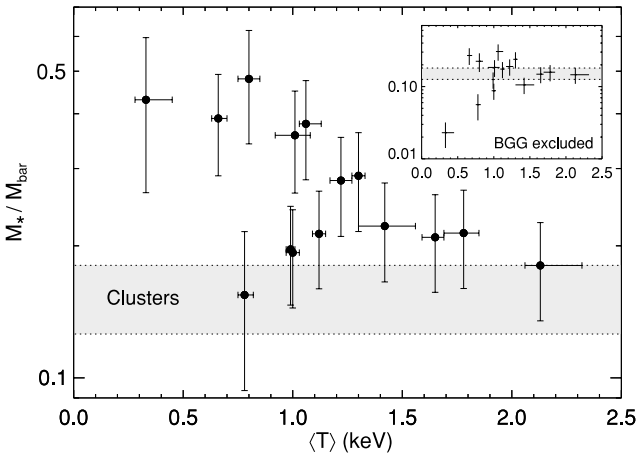

Figure 13. Stellar-to-baryon mass ratio inside r_{500}. The shaded region outlines the 1σ range of $M_*/(M_* + M_{\rm ICM}) = 0.16^{+0.02}_{-0.03}$ covered by the clusters of Ettori (2003). Inset shows the corresponding result (same units) with the contribution from the BGG excluded.

as the possibility that the stellar population has simply produced systematically fewer metals in cool groups; the metallicity of the stellar population is typically at least $\sim$ solar in many of the bright early types in our groups, with no obvious differences from central cluster galaxies (see e.g. Humphrey & Buote 2006; Brough et al. 2007). However, it is also clear that the moderate trend of decreasing cold fraction with T is largely driven by the BGG (see inset in Fig. 13). If considering the contribution to $M_*/M_{\rm bar}$ from satellite galaxies alone, there is no systematic variation with group temperature ($|\sigma_{\rm K}| = 0.3$, regardless of whether NGC 2300 is included), and most groups are then consistent with the corresponding cluster results.

For a fixed baryon fraction, a higher cold fraction in low-mass systems is perhaps no surprise. Cooler systems have lower characteristic entropies (Ponman, Sanderson & Finoguenov 2003) and hence cooling times (Sanderson, Ponman & O'Sullivan 2006), and so a larger fraction of their hot gas can be expected to cool out. As discussed by Gonzalez et al. (2007), a higher galaxy/SF efficiency in low-mass systems could also be promoted by an increased efficiency of tidal interactions (boosting star formation rates (SFRs)) and a decreased efficiency of strangulation, i.e. the stripping of any gas halo of late-type galaxies.

It is nevertheless interesting to note that, if accounting also for the iron locked in stars, a *higher* $f_{\rm c}$ in cool systems could potentially maintain a *total* IMLR comparable to that seen in clusters. However, it seems that only the stellar population of the BGG itself could likely provide any significant modifications to a trend in this total IMLR with T, because Fig. 13 shows that the stellar metal contribution from satellite galaxies would not vary systematically with T unless stellar metallicity does. For the sake of argument, we note that any correlation of total IMLR with $\langle T \rangle$ can be made to vanish for our sample provided that the stellar population in the BGG has mildly supersolar metallicity, [Fe/H] $\approx +0.2$ in all groups. While not an unreasonable assumption (see e.g. Humphrey & Buote 2006), the resulting mean total IMLR of $\sim 7 \times 10^{-3}$ would still be a factor of $\sim$3 below the corresponding value for clusters (which is $\sim$0.02 for our adopted abundance table; Renzini 2004). The contribution from satellite galaxies can raise this mean, but restores the temperature dependence, unless the (mass-weighted) mean stellar metallicity declines from $Z_{\rm Fe} \sim 2\,Z_\odot$ to $\sim$ solar across our temperature range. In other words, a higher $f_{\rm c}$ in cooler groups

can only keep the *total* IMLR independent of T and in accordance with cluster values while maintaining the trends in Fig. 8 if a much larger fraction of synthesized metals remains locked in stars in cool systems. Although we lack the data to exclude this with confidence, it seems unlikely for several reasons, in part because it requires considerable systematic variation in SF histories and/or IMF and stellar binary fraction among the bright early types in cool and hot groups. Secondly, a higher average stellar metallicity in cooler groups – in which the average galaxy stellar mass is lower, as discussed below – would conflict with the well-established local mass–metallicity relation, which appears fairly insensitive to environment (e.g. Bernardi et al. 2003).

Including the contribution of any IC stars in our groups could help explain the trends in Fig. 13, if such a component is more prominent in poorer systems as suggested by Gonzalez et al. (2007). However, given that its estimated contribution to the stellar mass in clusters is still of the order of ∼30 per cent (see Section 4.2), it seems improbable that it can account for the order-of-magnitude variation in $M_{\rm gas}/L_B$ among our groups, nor would it explain the seriously reduced IMLRs in cool systems. In summary, it seems clear that a systematically varying galaxy formation efficiency, or even a contribution from stars not included in our estimates of L_B or M_*, cannot account for the results in Fig. 8. Given the higher cold fraction in cooler systems, one would naively expect higher ICM abundances in these, at variance with our results.

Although a varying SF efficiency cannot explain the trends in Fig. 8, it is still instructive to also explore the potential role of variations in average SF *history* among the groups. For example, is it conceivable that ICM enrichment has somehow been sufficiently 'delayed' in lower mass systems to help explain their lower IMLR? To investigate this, we show in Fig. 14 the mass-weighted Si/Fe ratio of the groups as a function of the corresponding Fe abundance, both restricted to radii $r \leq 0.5r_{500}$ inside which we have reliable measurements for all 15 groups. Systems have been grouped according to their mean temperature. Nominally, the data show a negative correlation with $Z_{\rm Fe}$ at the 2.0σ level, suggesting a higher Si/Fe and lower overall Fe abundance in cooler groups within these radii. The statistical errors are large, however, clearly exceeding the systematic variations, so the results have also been accumulated in three temperature bins for clarity, as illustrated in the figure inset. This confirms the initial impression, demonstrating that the ICM in cooler and less enriched groups tends to contain a relative preponderance of SN II ejecta.

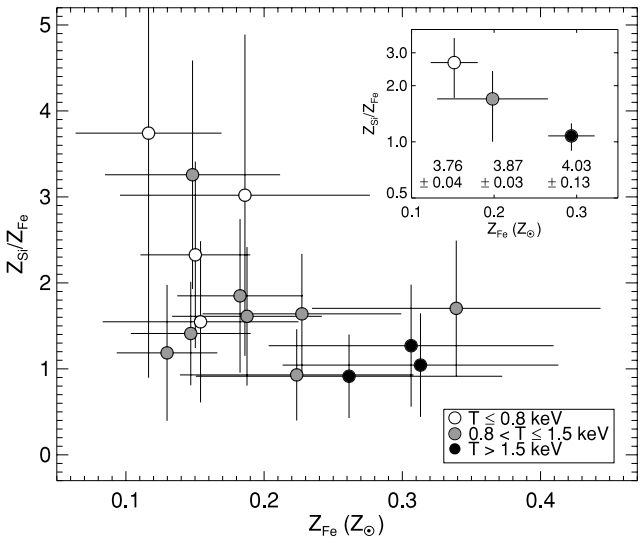

Figure 14. Mass-weighted Fe abundances and Si/Fe ratios within $0.5r_{500}$. Systems are colour-coded according to their $\langle T \rangle$ as labelled. Inset shows mean results within the temperature bins, with uncertainties reflecting the mean and standard deviation within each bin. Annotations in inset provide the mean total B–K colour within r_{500} and its 1σ error for the group members within each bin.

In analogy with stellar population studies, the tendency for the ICM to be less Fe-enriched and display higher α/Fe ratios in cooler groups suggests a chemically 'younger' ICM in these groups. On average, galaxies also tend to be slightly bluer in the cooler groups, as indicated in the figure inset, and furthermore are less massive, with the average stellar mass from equation (2) showing a positive correlation with $\langle T \rangle$ at 3.0 and 3.4σ significance for BGGs and satellites, respectively. While several explanations may be possible for these results, the data are at least consistent with a scenario in which the (generally bluer and less massive) galaxies in our cooler groups have experienced slightly more extended SF histories, whereas the conversion of the available gas into stars was completed earlier in the more massive galaxies in hotter groups. As a consequence, SF and metal production (from SN Ia in particular) might be progressively 'delayed' in lower mass systems.

Although these results should be regarded as tentative ($\sigma_{\rm K} = -1.3$ for a correlation between $Z_{\rm Si}/Z_{\rm Fe}$ and total $B - K$ colour), they could be a manifestation of the observation that more massive early-type galaxies tend to be older, i.e. have completed the bulk of their SF (and the associated ICM enrichment by SN II and stellar winds) at higher redshift ('downsizing'; e.g. Cattaneo et al. 2008), as well as an effect by which such galaxies at fixed mass tend to be slightly older in more massive environments (e.g. Sánchez-Blázquez et al. 2006), perhaps indicative of an environmental dependence of downsizing. This interpretation is also in accord with the inference of Loewenstein (2006) that the fraction of baryons processed through stars is lower in lower density environments compared to in rich clusters. Nevertheless, the inferred average colour variations between galaxies in the cool and hot groups are small, $\Delta(B - K) \lesssim 0.3$, so it remains highly questionable whether average SF histories have varied sufficiently with group mass to explain the observed order-of-magnitude variation in IMLR from both SN Ia and SN II.

In conclusion, it seems unlikely that arguments invoking changing SF efficiencies *or* histories with group mass can themselves explain the results in Fig. 8. The above results are, on the other hand, consistent with, for example, substantial gas (and hence metal) loss from within r_{500} in lower mass systems. In fact, the simulations of Davé et al. (2008) indicate that the higher cold fraction in cool systems (which, naively, could be expected to result in higher ICM metal abundances) is compensated for by galactic outflows that drive more metals out of the potentials of cooler systems. We consider this possibility in Section 4.4.

4.2 Metal release efficiency

Metals can be released into the ICM through several mechanisms, including galactic outflows, stripping of enriched material by galaxy–galaxy and galaxy–ICM interactions, and direct *in situ* enrichment by IC stars. Here we consider these mechanisms in turn, posing the question of whether metals have been released less efficiently into the ICM in cooler groups. One immediately attractive feature of this possibility is its potential to account for the lower metal mass-to-light ratios of both SN Ia and SN II products. For example, gaseous stripping would likely affect both SN Ia and SN II products, and tidally stripped IC stars should release both SN Ia and

SN II metals with equal efficiency. In addition, any metal release mechanism whose efficiency scales with system temperature might alleviate the need for a redshift-dependent SN Ia rate in the BGG (Section 3.4), and help explain the observed *Z*–*T* trend in group cores.

4.2.1 Galactic outflows

Some fraction of all metals released by SN in the group members will never mix with the ICM but will remain in the parent galaxy and potentially participate in subsequent SF. Fig. 8 then raises the possibility that SN ejecta were released less efficiently into the ICM in cooler systems. To evaluate the feasibility of this scenario, we can compare the total SN energy inferred from the ICM abundance pattern $E_{\rm SN,ICM}$ (Fig. 11) to that expected from the stellar population within a group, $E_{\rm SN,*}$. Naively, one would expect $\eta = E_{\rm SN,ICM}/E_{\rm SN,*} \lesssim 1$, the exact value depending on the mass fraction of SN ejecta retained by the galaxies.

For each group, $E_{\rm SN,*}$ can be estimated from the stellar mass of the group members, noting that a Salpeter IMF with an assumed minimum mass for core-collapse progenitors of 8 $M_\odot$ implies one core-collapse SN per $\sim$150 $M_\odot$ of stars formed. In addition, a typical stellar α/Fe ratio of $\sim$ solar in the group members (Humphrey & Buote 2006) implies that at least $\sim$0.3 SN Ia must have exploded for each SN II. Adding these numbers yields $E_{\rm SN,*} \sim 9 \times 10^{48}$ $(M_*/M_\odot)$ erg, and the resulting comparison to $E_{\rm SN,ICM}$ within r_{500} is plotted in Fig. 15. With a resulting sample mean and 1σ error of $\eta = 0.68 \pm 0.10$, our numbers are in broad agreement with existing theoretical and observational estimates of the mass loss fraction of galaxies, which range from $\eta \approx 0.4$ to 0.8 (see e.g. Sivanandam et al. 2009 and references therein). In particular, as illustrated in Fig. 15, the latter authors find a value of $\eta = 0.84^{+0.11}_{-0.14}$ within r_{500} in clusters using an approach based on the observed SN Ia rate in cluster early types, while noting that the fraction could be as low as 35 per cent if the assumed SN rates were increased to within their 2σ upper limit.

Interestingly, while this suggests that ICM enrichment has been fairly efficient for our sample as a whole, there *is* also a tendency ($\sigma_{\rm K} = +1.7$, rising to +2.5 if excluding the outlying NGC 2300) towards higher η in hotter groups. This result could be anticipated from Figs 11 and 13: since the estimated $E_{\rm SN,ICM}$ per ICM particle does not vary systematically with T, the trend in Fig. 15 is a consequence of the systematic decrease in cold fraction with T. The result is consistent with the notion that SN products have been released more efficiently into the ICM in hotter systems, although other explanations are possible. These include the possibility of the stellar IMF and/or mean metallicity varying systematically with T, as this would lead to systematic variations in the predicted number of SN per stellar mass and in the estimated stellar mass itself.

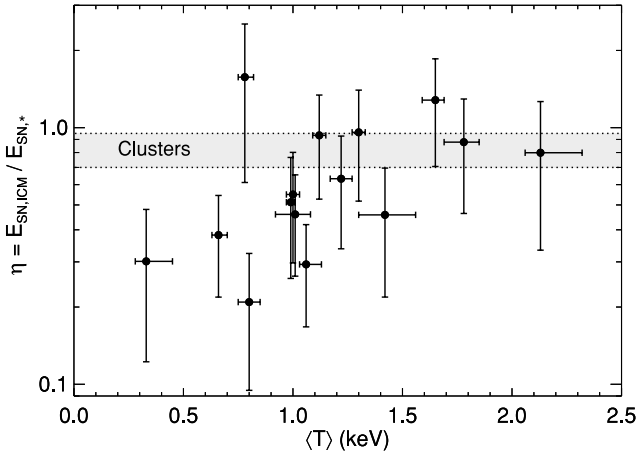

Figure 15. Ratio of SN energy released in the groups as inferred from ICM abundances to that expected from the stellar mass of the group members. Shaded region marks the estimate for the $T \approx$ 2–6 keV clusters of Sivanandam et al. (2009).

Nominal values of η exceeding unity are seen in a few cases, but all results are consistent with $\eta < 1$ even without accounting for uncertainties in SN rates and yields. Other possible effects include the presence of optically undetected IC stars, which would contribute to $E_{\rm SN,ICM}$ only, and more speculatively the possibility of pre-enrichment, whereby some of the ICM material accreted by the groups was enriched by galaxies not currently in the group. In addition, we cannot exclude that ICM masses may be slightly overestimated in some groups, nor that the SN Ia contribution to $E_{\rm SN,*}$ may be underestimated (cf. Sivanandam et al. 2009). The fact that η is not constant and generally *different* from unity is no surprise though. As pointed out by Davé et al. (2008), X-ray emission-weighted α/Fe ratios, used here to infer $E_{\rm SN,ICM}$, may not be a good indicator of the relative number of SN Ia and SN II that have exploded within the group, but rather reflects the metal distribution mechanisms at work.

A possible interpretation of the systematic trend in Fig. 15 is that SN-driven outflows have been more efficient at releasing metals into the ICM in hotter groups. Whether this might be expected on the basis of the higher average galaxy mass in such groups is not immediately obvious though. A deeper galactic gravitational potential might disfavour the development of a freely outflowing starburst wind, but, conversely, SF may generally have proceeded more rapidly and vigorously in massive galaxies. An alternative explanation invokes the possibility of AGN-driven outflows helping to release metals into the ICM. Observational evidence for such outflows to exhibit significantly supersolar abundances for a range of elements has been reported (Arav et al. 2007; Wang et al. 2007), and numerical simulations (Moll et al. 2007) indicate that AGN outflows could contribute significantly to cluster enrichment.

Since most of our groups show some evidence of ongoing or recent AGN activity (Paper I), the relevant question is whether such activity, and its impact on the ICM, scales with $\langle T \rangle$ as required by Fig. 15. More specifically, since AGN activity may expect to scale with stellar bulge mass of the host galaxy, we can test whether the trend in Fig. 15 is explicable on the basis of higher BGG bulge masses in hotter groups. Adopting again the distinction between cool and hot groups introduced with Fig. 9, we note that η is significantly higher in hotter ($T > 1.1$ keV) groups by 58 $\pm$ 18 per cent. Using the BGG central stellar velocity dispersions $\sigma_{0,*}$ listed in Table 2 we find some tendency for these to increase systematically with T at the same level of significance as that of η versus T ($\sigma_{\rm K} = +1.7$). However the trend is considerably flatter than that of $\eta(T)$, with results showing a mean and 1σ error of $\langle \sigma_{0,*} \rangle = 267 \pm 15$ and 278 ± 10 km s^{-1} for cool and hot groups, respectively, indistinguishable at the 1σ level. Qualitatively similar results are obtained for $\langle \sigma^4_{0,*} \rangle$, which is expected to scale with the mass of the central supermassive black hole (SMBH) (Ferrarese & Merritt 2000; Gebhardt et al. 2000). In other words, there are no indications that central black hole masses are generally higher in hotter groups, and this result still ignores the fact that relatively more gas needs to be enriched in more massive systems. Hence, unless more massive black holes are considerably more efficient *for their mass* at expelling metals from their host bulges, these considerations suggest

that the trend in Fig. 15 is not driven by increased AGN activity in hotter groups, at least not if associated with the BGG only.

4.2.2 *Stripping and interactions*

Gas and metal loss from galaxies induced by interactions with the ICM could also help explain the trend in Fig. 15. An indication that some (presumably enriched) gas has been removed from our group galaxies by other means than SN outflows is provided by the factor of 2–3 deficiency in HI mass derived for the spirals in NGC 5044 and NGC 7619 compared to field spirals of similar optical morphology and size (Sengupta & Balasubramanyam 2006). In addition, evidence for ongoing or past stripping associated with galaxy–ICM interactions is present in a few of our groups (Rasmussen, Ponman & Mulchaey 2006; Mendel et al. 2009). General support for this interpretation comes from the work of Finoguenov et al. (2006) who find a larger scatter in metallicity than in entropy in the group cores within their sample, which they interpret as evidence for diversity in the origin of gas in the cores. On the other hand, Renzini (2004) notes that if, e.g., ram pressure stripping were important for ICM enrichment, then hotter clusters with higher galaxy velocity dispersion should show relatively higher ICM abundances. While this is not observed in his results, nor in those of Baumgartner et al. (2005), such a trend *is* seen for our sample, and, interestingly, is confined to the regions of highest ICM density (Fig. 10).

This trend is certainly consistent with a density-dependent metal release mechanism in group cores, whose efficiency scales with galaxy velocity dispersion. If ram pressure stripping is the culprit, we might expect the ICM abundance in the central region to scale more strongly with the characteristic ram pressure in this region than with group temperature. In order to test this possibility, the velocity dispersion σ_v of each group (Table 1) was used to estimate the characteristic ram pressure within $0.1r_{500}$. Assuming $P_{\rm ram} = (M_{\rm gas}/V)\sigma_v^2$, with $V = (4/3)\pi\ (0.1r_{500})^3$, we find evidence for a moderately significant correlation between $P_{\rm ram}$ and the mass-weighted Fe abundance within $0.1r_{500}(\sigma_K = +2.1)$, though the correlation of $Z_{\rm Fe}$ with $\langle T\rangle$ is actually stronger ($\sigma_K = +2.6$ for own groups, +3.0 when including those of Finoguenov et al. (2006, 2007) as discussed in Section 3.2). In addition, the corresponding correlation of $Z_{\rm Si}$ with $P_{\rm ram}$ is weak ($\sigma_K = +1.1$ compared to +2.5 for $Z_{\rm Si}$ versus $\langle T\rangle$). While keeping in mind that the estimated σ_v may not always be representative of the typical 3D galaxy velocity in each group if affected by velocity anisotropies or small-number statistics (although 13 out of our 15 groups have more than 10 members), we thus find that results are consistent with ram pressure stripping contributing to enrichment in group core, but the evidence is tentative at best, and we cannot rule out other density-dependent mechanisms as more important. Moreover, as this process should be inefficient at large radii (and where, indeed, no clear trend in Z with T exists), we conclude that the reduced efficiency of stripping through galaxy–ICM interactions in cooler systems is unlikely to account for their lower IMLRs or for the trend in Fig. 15.

Note that if the metallicity–temperature trend in group cores does reflects an increased efficiency of environment-driven gas loss from galaxies in hotter groups, then the absence of a similar trend in systems with $T \gtrsim 3$ keV (De Grandi et al. 2004) may suggest that such processes 'saturate' at $T \sim 2$–3 keV, perhaps as a consequence of near-complete gas removal from core galaxies in clusters above these temperatures. It is yet to be established to what extent this possibility is in accord with simulation results, which suggest that only a minor fraction (∼10 per cent) of the global ICM metal budget even in massive clusters can be accounted for by ram pressure stripping, though with the fraction considerably higher in cluster cores (Domainko et al. 2006; Kapferer et al. 2007).

Other interaction processes involve galaxy–galaxy interactions such as harassment, tidal interactions and mergers. The latter process in particular may also release metals to the ICM, in part because a significant fraction of a galaxy's ISM may shock-heat and become unbound during major mergers, and in part because the merger activity may further trigger a starburst- or AGN-induced outflow (e.g. Cox et al. 2006; Hopkins et al. 2006). Our data do not allow useful constraints on the contribution of this process to ICM enrichment, however, and cosmological simulations may still lack the dynamic range to robustly assess whether it has been substantially less efficient or influential in low-mass systems compared to clusters. Naively, one would expect tidal stripping and mergers to be more effective in poorer systems owing to the lower velocity dispersion, suggesting that these mechanisms cannot explain the trends in Figs 8 and 15.

4.2.3 *Enrichment by intracluster stars*

IC stars represent a non-negligible component of the baryons in groups and clusters, and could pollute the ICM very efficiently since their ejecta are released directly into the ICM. Observations suggest that ∼30 per cent of the stellar mass in clusters within r_{500} may be contained in IC stars (Gonzalez et al. 2007), but it remains debatable whether this fraction decreases with total cluster mass as claimed by Gonzalez et al. (2007), or rises asymptotically with mass to a level of ∼50 per cent of M_* as suggested by other observational and theoretical studies (Lin & Mohr 2004; Conroy, Wechsler & Kravtsov 2007; Purcell, Bullock & Zentner 2007).

Since this component is not accounted for in the cluster comparison results in Figs 7 and 8, including its contribution to L_B could affect the apparent group-cluster discrepancies. For example, if IC light is less prominent in cooler systems as suggested by some of the above results, this could help explain the lower ICM abundances in groups. However, even a 50 per cent increase in IC stellar light in massive clusters is insufficient to bring the lower group IMLR within the factor of 2 of rich clusters that is explicable on the basis of the lower large-radius abundances in groups. Furthermore, Sivanandam et al. (2009) conclude that 20–25 per cent of the Fe in the ICM within r_{500} can be accounted for by IC stars, implying that IC stars contribute in roughly equal proportions to the stellar mass and ICM Fe enrichment in clusters. This suggests that the resulting IMLR should not be significantly affected by the presence of this component. Consequently, it seems we can exclude the possibility that IC light provides an important contribution to the trends in Fig. 8. This would be particularly true if this component is actually more important in cooler systems, as suggested by Gonzalez et al. (2007).

IC stars could still play an important role for ICM enrichment in group cores, however. A relevant question is whether the metal contribution from these can alleviate the need for a redshift-dependent SN Ia rate in the BGG to account for the Fe within the cool core (cf. the discussion of Fig. 12). Where IC light in clusters can be separated from that of the central galaxy, the former typically contributes ∼80 per cent of their combined optical output within r_{500} (Sivanandam et al. 2009). This fraction will be lower inside $0.1r_{500}$, because IC light is more widely distributed than that of the BGG. For simplicity, if assuming that the IC light traces the group gravitational potential and that its K-band luminosity density is distributed

according to an NFW profile (Navarro, Frenk & White 1997) with a typical concentration $c = 5$–10, then 5–10 per cent of this light would fall inside $0.1r_{500}$. The implication is that this component can potentially reduce the enrichment times in Fig. 12 by a factor of $\sim$1.4 (optimistically assuming a total K-band contribution of four times that of the BGG, of which 10 per cent falls within $0.1r_{500}$). Although this factor assumes that none of this light is already accounted for in the adopted values of $L_{\rm K,BGG}$, it may still be large enough to eliminate the need for an evolving BGG SN Ia rate, especially if the IC contribution does increase with group mass. What IC stars probably *cannot* do, however, is account for the observed Z–T trend in group cores (Fig. 10). Even if the fractional Fe contribution from IC stars within $0.1r_{500}$ increases by 50 per cent across our temperature range (at variance with the Gonzalez et al. 2007 results), this would still fall an order of magnitude short of explaining the factor $\sim$10 rise in $Z_{\rm Fe}$ within this radius. Arguments invoking a far superior enrichment efficiency from this component (compared to stars in galaxies) would also fail, since Fig. 15 suggests that galaxies are already fairly efficient in polluting the ICM.

4.3 Cooling of enriched gas in group cores

Turning now to the possibility that metals were *removed* from groups rather than not produced or released into the ICM, we first consider a scenario in which radiative cooling has removed enriched gas from the X-ray phase. At a given fraction of r_{500}, cooling times tend to be lower in cooler systems (e.g. Sanderson et al. 2006), so this explanation would be consistent with such systems exhibiting lower $M_{\rm gas}/L_B$ and missing relatively more metals, as suggested by Figs 7 and 8. The process is nevertheless still limited by the observation of the central abundance excess, because cooling rates above a certain threshold would eventually destroy the central excess due to the associated inflow of less enriched material from larger radii.

Radiative cooling would primarily deplete SN Ia products, due to their higher concentration at small radii where cooling is most rapid. Thus, the two questions we seek to address is whether the amount of Fe generated by SN Ia that is 'missing' in Fig. 8(h) (or its K-band analogue) can be accounted for by cooling, and whether that would ultimately destroy the central Fe excess in conflict with our observations. Since Figs 8 and 13 indicate that the properties of our most massive group, the $T \approx 2.1$ keV system NGC 6338, are fairly representative of those of more massive clusters, we can use this group as a benchmark for characterizing deviations in cool systems from cluster results. On the basis of the K-band $\rm IMLR_{Ia}$ in NGC 6338 deduced from Table 1, we evaluated the missing Fe mass in each group and hence the corresponding total missing gas mass for a given assumed Fe abundance of the cooled-out gas. Making the assumptions that the gas cooling out had $Z \approx \rm Z_\odot$ as observed in the group cores and, conservatively, that this gas has been cooling for 10 Gyr (corresponding to an initial redshift of $z = 2$ for the adopted cosmology), resulting mean cooling rates could be computed.

Fig. 16(a) shows the required cooling rates as a function of mean group temperature, demonstrating that modest average rates of a few tens of $\rm M_\odot\ yr^{-1}$ would be necessary under the above assumptions. Note that NGC 6338 itself has not been included in the plot, nor has the $\langle T\rangle \approx 1$ keV system NGC 4325, which actually exhibits a slightly higher K-band $\rm IMLR_{Ia}$ than NGC 6338 and so is not Fe-deficient according to our assumptions. Of course, the derived rates assume that gas in group cores was already enriched to solar levels by $z \approx 2$ and has been subject to unimpeded cooling ever since. These estimates are thus likely representing a best-case scenario, and the total missing gas mass becomes correspondingly larger if

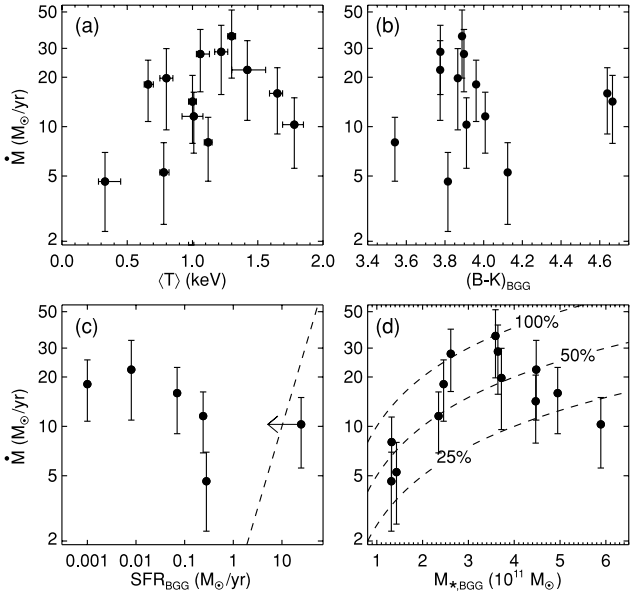

Figure 16. The time-averaged gas cooling rate $\dot{M}$ required to account for the shortfall of $\rm IMLR_{Ia}$ compared to NGC 6338, assuming cooling over a 10 Gyr time-scale. Results are plotted as a function of (a) $\langle T\rangle$, (b) the B–K colour of the brightest group galaxy, (c) the SFR of the latter, where available (see text for details) and (d) the stellar mass of the latter. Dashed line in (c) represents equality, while lines in (d) mark out constant fractions of cooled-out gas mass relative to the stellar mass of the BGG, with fractions as labelled. Uncertainties on $\dot{M}$ reflect the relative errors on $\rm IMLR_{Ia}$.

assuming a lower $Z_{\rm Fe}$ for the removed gas. For example, adopting instead the current $M_{\rm Fe}/M_{\rm gas}$ ratio within r_{500} in each group as representative of the assumed Fe content of the cooled-out gas, the required $\dot{M}$ rises to a sample mean of $\sim 130\,\rm M_\odot\ yr^{-1}$. Such values seem prohibitively large at present, but we cannot a priori exclude cooling rates of this magnitude in the past. Note also that cooling should be more efficient in lower T systems, and although Fig. 16(a) indicates a weakly significant tendency ($\sigma_{\rm K} = +1.2$) towards higher cooling rate requirements in hotter systems, there is a clear negative trend with T if normalizing the required $\dot{M}$ by the total gas mass ($\sigma_{\rm K} = -2.6$) or gravitating mass ($\sigma_{\rm K} = -2.1$, assuming $M_{\rm grav} \propto T^{3/2}$) of the group.

Although the central temperature is not observed to drop below $\sim$40 per cent of the peak value in any of the groups (Paper I), it is still relevant to ask whether there are any indirect signs of *ongoing* strong cooling where this is most needed. If central cooling is currently proceeding at the required rates, and some of the cooled-out gas participates in SF, one might expect systematically bluer BGGs in higher $\dot{M}$ groups. We investigate this in Fig. 16(b), which reveals no significant dependence between $\dot{M}$ and BGG colour ($\sigma_{\rm K} = -0.7$), not even if normalizing required $\dot{M}$ by $L_{\rm K}$ of the BGG ($\sigma_{\rm K} = -0.5$). For the galaxies with the relevant available data, we can be more specific and compare the required $\dot{M}$ to the current central SFR, noting that some low-level 'residual' SF seems to be taking place in many nearby early-type galaxies (e.g. Combes, Young & Bureau 2007). Hence, unless cooling and SF are highly episodic, one might again expect a correlation between $\dot{M}$ and current SFR. We have used available Hα and ultraviolet (UV) data from the literature to test this scenario (again excluding NGC 4325 and 6338). Hα-based SFRs from SDSS-DR4 data (Brinchmann et al. 2004) were adopted for NGC 4073 (the BGG in MKW 4) and NGC 5846, while Hα fluxes were taken from NED for NGC 383 and 741 (Capetti, Verdoes

Kleijn & Chiaberge 2005), and UV fluxes from NED for NGC 1407 (Rifatto, Longo & Capaccioli 1995) and NGC 4125 (Dale et al. 2007). For the latter four galaxies, SFRs were estimated using the relations of Kennicutt (1998), which should be sufficiently accurate for our purposes. The UV luminosities have been corrected for Galactic extinction but not internal dust extinction, which should be small for these early types. The Hα fluxes typically derive from the central galaxy regions, so some AGN contribution is possible in these cases. For example, the Hα emission from NGC 4073 cannot be unambiguously classified as either due to SF or an AGN, so we have treated this result as an upper limit. The results are plotted in Fig. 16c and show, if anything, a trend that runs opposite to expectations in our cooling scenario, and with SFRs generally several orders of magnitude below the required cooling rates.

Thus, we find no convincing evidence that the required central cooling in the groups is associated with any recent SF in the BGG, with the necessary cooling rates generally higher than even current SFRs in central galaxies of 'cooling flow' clusters (these rarely exceed 5–10 $M_\odot\,yr^{-1}$ and are often much smaller; cf. Rafferty et al. 2006). This is corroborated by the fact that there is no clear tendency for the BGG to be bluer in cooler systems ($\sigma_K = -0.4$) where cooling is expected to be more efficient. Further, large amounts of recent cooling-induced SF seems incompatible with the inferred ages of the stellar population in many of the BGGs, which are of order 10 Gyr (e.g. Humphrey & Buote 2006). This issue can potentially be circumvented in the – perhaps somewhat unlikely – event that much of the cooled-out gas has been deposited without participating in SF. If so there should be substantial (several $10^{10}\,M_\odot$) reservoirs of cold gas residing in the group cores, but H I measurements listed in NED, where available, only reveal upper limits, with NGC 5846 as the only exception.

The above considerations argue against significant recent cooling, and reveal no indications that ongoing cooling is more important where required. However, this does not preclude the possibility of stronger cooling activity in the past, where it could have contributed to building the current stellar mass of the BGG. If so, and if cooling is indeed responsible for removing metals, one might expect the stellar mass $M_{*,BGG}$ of the central galaxy, and the ratio of this to total ICM mass within r_{500}, to correlate positively with the required amount of cooled-out gas. This is not clearly the case though, with correlation significances of only $\sigma_K = +1.3$ and $+0.1$, respectively. An example is demonstrated in Fig. 16(d), which compares $\dot{M}$ to $M_{*,BGG}$. In a few cases, the required cooled gas mass nominally represents $\sim$100 per cent of the current stellar mass of the BGG (implying that the vast majority of the metals proposed to have cooled out cannot have been supplied by the BGG itself), while on average it corresponds to about half this value.

Although the latter case may not necessarily be completely at variance with the typical history of mass build-up and SF in these galaxies (which may still have assembled a significant fraction of their current stellar mass since $z \sim 2$), there is an additional and very powerful constraint on the allowing cooling rates arising from the presence of the central Fe excesses. As the typical estimated iron injection rate from the BGG is of order $\sim 0.02\,M_\odot\,yr^{-1}$ if including both SN Ia and stellar winds, the cooling rates implied by Fig. 16 would destroy the observed excesses on typical time-scales of only $\sim 10^7$ yr through the associated inflow of less enriched material from larger radii (while also flattening the central entropy distribution for the same reasons, although a discussion of this is beyond the scope of the present study). This severely compromises the viability of recent cooling as a mechanism to reduce the global X-ray IMLRs in cooler systems.

Could central cooling and inflow of low-Z gas still play a role for establishing the central Z–T trend in Fig. 10? If repeating the cooling calculations underlying Fig. 16 using the 'missing' metal mass inside $0.1r_{500}$ (again assuming that $IMLR_{Ia}$ in NGC 6338 is representative of the case of no missing metals), then the typical required cooling rates are a factor of $\sim$3 smaller, with some tendency for the required $\dot{M}/M_{gas}$ to decrease with T ($\sigma_K = -2.5$) and for $\dot{M}/L_{K,BGG}$($\sigma_K = -1.7$) to decrease with $(B-K)_{BGG}$. This suggests that central cooling could have played some role in removing metals from group cores and suppress the central Fe excess in the coolest systems, although, again, unimpeded cooling at the rates required to explain the Z–T trend within $0.1r_{500}$ in Fig. 10 would generally have destroyed the observed Fe excesses.

In summary, although cooling rates under optimistic assumptions *may* be sufficiently low in some systems for this mechanism to remain a viable means of removing some metals from the X-ray phase, the rates must generally be far below than those required to account for the global shortfall of Fe within r_{500} implied by Fig. 8. In addition, there are no clear indications that cooling is, or has been, more prominent in the systems with the largest deficit of SN Ia metals. As mentioned, cooling would also primarily affect SN Ia products, thus likely still requiring a separate mechanism to also account for the lower $IMLR_{II}$ in cooler systems. We thus conclude that central cooling cannot generally have been important in establishing the low IMLR of groups.

4.4 Recent gas and metal loss from groups

Another way to induce a lower IMLR in groups is through gas or metal loss from the potential wells of low-mass systems. This could help account for the lower gas mass-to-light ratios (via bulk gas loss) and potentially also the lower abundances (via preferential loss of highly enriched gas). As a means of discriminating between bulk gas loss and selective loss of enriched gas, we note that only the latter process would generally reduce the inferred abundances. The efficiency of such a mechanism should depend on group temperature, and our sample is large enough to allow a crude test for such an effect as demonstrated in Figs 9 and 10.

Beyond $0.5r_{500}$, Fe has mainly been produced by SN II (Fig. 6), so Z_{Fe} should here provide a crude measure of the ability of the systems to retain the products of starburst-driven galactic winds. There is little evidence from Fig. 10 that this ability varies systematically across the temperature range probed here ($\sigma_K < 1$), although the correlation significance rises to $\sigma_K = +1.2$ if excluding the fossil group NGC 741 which is extremely iron-deficient in the outskirts. Hence, although statistics at large radii are limited and dominated by the hotter groups in the sample, with only three systems from the 'cool' ($T \leq 1.1$ keV) subsample included in the last panel of Fig. 10, it seems clear that selective removal of enriched gas from cooler systems does not contribute significantly to the trends in Fig. 8. Moreover, given the strong radial decline of the mean Fe profile for the sample, a possible alternative – *bulk* gas loss from outskirts without preferential loss of metals – would predominantly have removed low-Z gas, thus leaving material with a *higher* abundance behind. Hence, while such a mechanism could have lowered M_{gas}/L_B in cool systems, it cannot account for the seriously reduced IMLRs in these environments.

Gas and metals can certainly still have been lost from groups. The absence of a clear temperature–abundance trend within 0.5–$1.0r_{500}$ could potentially be an artefact of small-number statistics and does not preclude the possibility that enriched gas has been expelled well beyond r_{500} in all systems. Any such activity might be ascribed to

galactic outflows driven by powerful SN or AGN activity, displacing ICM metals to radii where they would generally escape detection in these low-T systems. In the absence of significant mixing, highly enriched high-entropy material released by such outflows would rise buoyantly in the ICM until in entropy equilibrium with the surroundings. We here consider the feasibility of such a scenario for both SN- and AGN-driven outflows.

4.4.1 Supernova-driven winds

Supernova-driven galactic winds should generally be dominated by SN II products. Indeed, observations of extraplanar X-ray emission associated with hot gas around star-forming galaxies indicate significantly enhanced α/Fe ratios of 2–3 times the solar value (Strickland et al. 2004). The radial increase in the Si/Fe ratio seen for our groups outside the central galaxy is, in fact, only reproduced in simulations where the feedback scheme favours the ejection of SN II products from galaxies over those of SN Ia (see Tornatore et al. 2004; Romeo et al. 2006). This raises the interesting possibility that the radial increase in the Si/Fe ratio inferred for many of our groups may be explained by SN II-dominated material that has risen in the ICM to mix with it at radii corresponding to a significant fraction of r_{500}, and occasionally beyond. This rise could have occurred by means of buoyancy forces and/or bulk kinetic energy imparted to the gas. Since star-forming spirals tend to avoid group cores (Helsdon & Ponman 2003), these galaxies will typically already be surrounded by high-entropy gas, so convective displacement of the enriched ejecta to large radii may be inefficient and mechanical work energetically favoured for removing large amounts of gas from within r_{500}.

Stringent tests of this possibility are impeded by the fact that SN wind properties remain poorly established. In particular, detailed hydrodynamical simulations indicate that much of the wind fluid in an SN-driven outflow may escape the galaxy in a high-entropy phase that would be difficult to detect with current X-ray instrumentation (Strickland & Stevens 2000). To obtain a crude estimate of wind properties, we may consider the tail gas being lost from the NGC 2276 starburst galaxy, a member of the NGC 2300 group in our sample (Rasmussen et al. 2006). This material is likely to contain a significant contribution from starburst outflows, though possibly with some hot ISM and surrounding ICM mixed in. The entropy of this gas is $\sim$300 keV cm^2, although this figure is probably uncertain by a factor of $\sim$2 due to the unknown geometry of the tail along the line of sight. Taken at face value, this gas would rise due to convection to at least $r \sim 0.6r_{500}$ if assuming the adopted ICM density profile for the group. This consideration suggests that starburst wind material *can* rise to significant radii in the ICM by means of buoyancy, provided that mixing with the surrounding material is suppressed at least initially, e.g. by magnetic fields.

If SN II-enriched material from starburst winds has been preferentially lost from lower mass systems to generate some of the trends in Fig. 8, one would naively expect a positive correlation between $M_{\rm Si}/M_{\rm Fe}$ and $\langle T\rangle$. While Fig. 14 already suggests otherwise, we examine this possibility more directly in Fig. 17, again showing this ratio within $0.5r_{500}$ only, to avoid reliance on our temperature-independent abundance parametrizations. The results are compared to the analogous values derived by Sato et al. (2007) for the $T \approx$ 3–3.5 keV clusters AWM 7 and A1060 inside 0.35 and $0.25r_{180}$ ($\approx$0.6 and $0.4r_{500}$), respectively. Fig. 17 indicates that Si has *not* been preferentially lost from the cores of lower mass systems for the T-range probed here. To the contrary, there is mild evidence

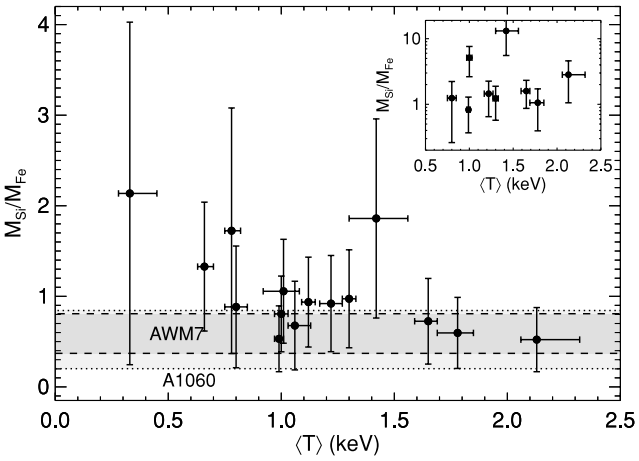

Figure 17. Ratio of silicon-to-iron mass inside $0.5r_{500}$. Also shown are the 90 per cent confidence intervals derived for the clusters AWM 7 (darker shade, dashed lines) and A1060 (lighter shade, dotted lines) by Sato et al. (2007). Inset shows the corresponding values within the range 0.5–$0.7r_{500}$ for the groups with data across this range.

for a negative correlation ($\sigma_{\rm K} = -1.8$), although this is driven by the three coolest systems, without which any correlation vanishes ($\sigma_{\rm K} = -0.3$). There is also no significant trend at larger radii ($\sigma_{\rm K} = +0.5$), as evidenced by the inset showing the corresponding results within 0.5–$0.7r_{500}$ for the nine groups with data extending across this range. Everything else being equal, buoyancy-driven bubbles of SN II material should be able to rise to larger radii in cooler (lower entropy) systems, but there is no evidence that the $M_{\rm Si}/M_{\rm Fe}$ ratio is higher at low $\langle T\rangle$ within this radial range. In other words, there is no clear evidence for a loss of SN II products from the central regions of cooler groups, nor for any such material to have been displaced to larger radii in those systems.

Comparison to the Sato et al. (2007) results thus suggests that any selective removal of SN II products from the central regions of low-mass systems by starburst winds must have occurred with comparable efficiency in systems with $T \lesssim 3.5$ keV, and so are unlikely to explain the trends seen for SN II products in Fig. 8. This conclusion is consistent with the results seen for the combined group–cluster sample of Finoguenov et al. (2000), which admittedly contains only four $T < 2$ keV systems. These authors find a roughly constant $Z_{\rm Si}/Z_{\rm Fe}$ ratio at $r = 0.2r_{180}$ for systems with a corresponding Si M/L ratio or gas mass fraction $f_{\rm gas}$ below a certain threshold. Above this value, the Si/Fe ratio appears to rise dramatically, with the transition occurring around Si $M/L \approx 0.01\,{\rm M}_\odot/{\rm L}_\odot$ or $f_{\rm gas} \approx$ 0.1, corresponding to $T \approx$ 3–4 keV (Finoguenov et al. 2001). One interpretation is again that metal loss due to starburst winds could be efficient in groups but that this process must have operated with near-uniform efficiency across the temperature range of our sample. While this may help to reduce ICM abundances in groups, it cannot, on its own, explain the SN II trends in Fig. 8, and much less so for the SN Ia products. On the basis of the available data, however, we cannot exclude the possibility that the discrepancy with respect to massive clusters could contain a contribution from this effect.

4.4.2 AGN-driven winds

The idea of central outflows driving material from group/cluster cores has received much recent attention with the observation that AGN in central cluster galaxies may be able to carve out cavities or bubbles in the surrounding ICM through radio outbursts (McNamara

& Nulsen 2007). Evidence of such activity has also been identified in small groups, including several of the systems within our sample (Allen et al. 2006; Morita et al. 2006; Jetha et al. 2008; Gastaldello et al. 2009). An indication that some AGN-induced gas mixing may have occurred in most, if not all, our groups is further provided by the radial extent of the central abundance excess, which is much broader than the distribution of optical light from the BGG (cf. Rebusco et al. 2006). Whether AGN-driven bubbles can rise far enough in clusters to displace large amounts of material from cluster cores remains unclear (e.g. Roediger et al. 2007), but semi-analytic models of galaxy formation have demonstrated that a variety of observational constraints in the group regime can be reasonably well satisfied in a scenario in which AGN may eject significant amounts of hot gas from low-mass haloes (Bower, McCarthy & Benson 2008). If so, AGN would provide an attractive explanation for the gas and metal deficiency evident for such systems in Fig. 8.

The standard assumption is that the observed cavities or bubbles have arrived at their current location mainly by means of buoyancy forces. If bubbles of enriched gas have travelled from group cores to beyond r_{500} by such forces only, the initial bubble entropy $S_0 = T/n_0^{2/3}$ must have been comparable to the ICM value S_{500} at r_{500}. We can evaluate the temperature difference corresponding to $\Delta S = S_{500} - S_0$ and hence the energy required to heat the relevant gas mass in group cores for it to be buoyantly displaced beyond r_{500}. In a similar vein to the previous section, we assume that the gas thus removed must account for the lower K-band $\mathrm{IMLR_{Ia}}$ in the groups when compared to NGC 6338. To treat all groups equally, we assume $T_{500} = 0.67\ \langle T\rangle$ for the ICM temperature at r_{500} (cf. Paper I, equation 7), along with $Z = \mathrm{Z_\odot}$ for the removed gas as observed in the group cores at present. For the initial entropy of the gas to be displaced, we note that inspection of our *Chandra* images of NGC 741, HCG 62 and NGC 5044, all groups with known X-ray cavities, suggests an average projected distance from the cavity centre to the optical centre of the BGG of roughly two-thirds of the D_{25} semi-major axis. Given our sample mean of ∼22 kpc for the latter, this estimate is in excellent agreement with the mean projected distance of ∼16 kpc seen for the radio-filled cavities in the combined group and cluster sample of Bırzan et al. (2004, see also Rafferty et al. 2006). We therefore evaluate the initial gas density and entropy at $r = 0.7D_{25}$.

Results are plotted in Fig. 18, in the form of the required heating energy ΔE. NGC 4325 and NGC 6338 itself are again excluded, for the reason discussed earlier. Most groups scatter within a factor of 2 in this plot, but NGC 2300 and 4125 are outliers due to their fairly high central entropies. The logarithmic mean of the heating energy corresponds to $E \approx 8 \times 10^{60}\ \mathrm{erg\ s^{-1}}$, with no significant dependence on $\langle T\rangle$ ($\sigma_\mathrm{K} = -0.1$) or $L_\mathrm{K,BGG}$($\sigma_\mathrm{K} = +1.5$). While such energy requirements may exceed typical AGN outburst energies inferred for local clusters (e.g. Rafferty et al. 2006), the required energy could have been deposited in the course of multiple outbursts, and so may be broadly consistent with existing observational estimates. We note, however, that the associated energy per total ICM particle is generally somewhat in excess of typical values required by preheating scenarios (mean of $\Delta E \approx 2.4$ keV particle^{-1}), and does show some evidence for a negative trend with $\langle T\rangle$ ($\sigma_\mathrm{K} = -1.8$) but not with $L_\mathrm{K,BGG}$($\sigma_\mathrm{K} = 0.0$).

These results suggest that the energetic requirements for displacing the required amount of gas and metals by buoyancy are generally large for the current ICM configuration, but perhaps not prohibitively so. Another way to arrive at this conclusion comes from considering the implied efficiency ϵ with which the central SMBH must have converted accreted mass into outflow energy, assuming that the released energy represents a converted rest mass corresponding to the current mass of the SMBH. Estimating central SMBH masses from the BGG central stellar velocity dispersions $\sigma_{0,*}$ listed in Table 2, using

$$M_\mathrm{BH} \sim 1.2 \times 10^8 \left(\frac{\sigma_{0,*}}{200\ \mathrm{km\ s^{-1}}}\right)^{3.75} \mathrm{M_\odot} \qquad (5)$$

(Gebhardt et al. 2000), we show the corresponding conversion efficiencies $\epsilon_\mathrm{BH} = \Delta E/M_\mathrm{BH}c^2$ in Fig. 18(b). Results fall in the range $\epsilon \sim 0.1$–5 per cent, with a median value of ≈1 per cent. Interestingly, but perhaps coincidentally, this is in broad agreement with recent estimates of the actual SMBH efficiency in converting accreted rest mass into outflow energy, $\epsilon \approx 0.5$–2 per cent (e.g. Allen et al. 2006; Merloni & Heinz 2008).

Further insight can be gained from comparing the required time-averaged heating power $\langle P\rangle$ to estimates of the current mechanical AGN output in the groups. Fig. 18(c) shows the mean power associated with the derived ΔE for a conservative assumption for the energy injection time-scale of 10 Gyr (again corresponding to an initial redshift $z \approx 2$). Fig. 18(d) compares this to rough estimates of the currently available power, based on the 1.4 GHz radio power $P_{1.4}$ of any central radio source as listed in Table 2. We converted $P_{1.4}$, where available, into current mechanical AGN power $L_\mathrm{mech} \approx 10^{25} L_\mathrm{radio}^{0.44}$, assuming $L_\mathrm{radio} \approx (8.6 \times 10^9\ \mathrm{Hz})\ \mathrm{P_{1.4}}$ as is appropriate for a power-law radio spectrum of index unity (Bîrzan et al. 2004). Results reveal that current central AGN activity in the groups is typically an order of magnitude weaker than the inferred time-averaged power required to accomplish the necessary gas removal. It is conceivable, however, that this may at least partly be related to selection effects, since any system with a powerful active radio

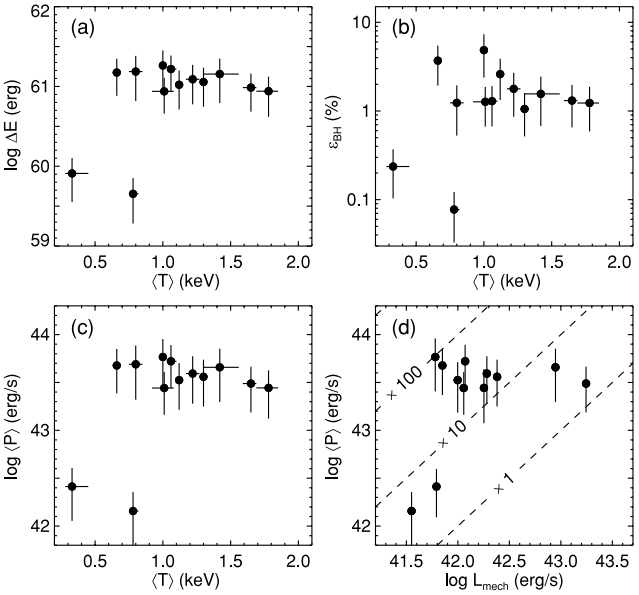

Figure 18. (a) Energy required to heat enriched gas in the group cores sufficiently for convection to carry this gas beyond r_{500} and so achieve the same $M_\mathrm{Fe}/L_\mathrm{K}$ ratio for SN Ia products within r_{500} as in NGC 6338. (b) The corresponding required black hole energy conversion efficiency for the estimated BGG black hole masses. (c) The corresponding time-averaged heating power $\langle P\rangle$ assuming an energy injection time of 10 Gyr. (d) As (c), but compared to the estimated current mechanical power L_mech of the central AGN, with typical constant $\langle P\rangle/L_\mathrm{mech}$ ratios marked by dashed lines. Uncertainties reflect the fractional errors on $\mathrm{IMLR_{Ia}}$.

source strongly disturbing the ICM might not have made it into our sample, which only includes groups which appear reasonably undisturbed on large scales in *Chandra* data.

While acknowledging that the estimates in Fig. 18 result from rather simplistic considerations which, among other things, ignore the potential contribution from AGN not associated with the BGG, the derived energy requirements suggest that some buoyant displacement of gas to beyond r_{500} by AGN activity may have taken place in the recent past, but the majority of any such activity is likely to have occurred when the ICM entropy configuration was more conducive to blow-out. Also note that our energy estimates are based on total mass losses assuming solar abundances for the removed gas, but that larger amounts of gas (and hence lower metallicities and larger outflow energies) would be needed if AGN were to also explain the *general* shortfall of hot gas compared to clusters evidenced by Fig. 13. In combination, this argues in favour of gas and metal loss predominantly, but not necessarily exclusively, at earlier epochs, closer to the redshift peak of metal production and possibly prior to group collapse.

We do note, however, that recent AGN outflows could easily have displaced highly enriched gas from group cores and so have contributed to the central Z–T trend in Fig. 10. Using similar assumptions as those underlying Fig. 18 but only considering the 'missing' Fe mass within $0.1r_{500}$ as derived from the data in Fig. 12(a), and assuming that this gas has simply been expelled beyond $0.1r_{500}$, the resulting energy requirements display sample mean values of $\langle \log \Delta \mathrm{E} \rangle \approx 59.6$ erg, $\langle \eta_{\mathrm{BH}} \rangle \approx 0.1$ per cent, $\langle \log \mathrm{P} \rangle \approx 42.1\,\mathrm{erg\,s^{-1}}$ and $\langle (\log \mathrm{P})/(\log P_{\mathrm{mech}}) \rangle \approx 1.0$. These requirements appear perfectly reasonable, and suggest that current AGN power in the groups is generally sufficient to buoyantly displace the required amount of enriched gas from within $0.1r_{500}$. The requirements are generally slightly harder to satisfy in hotter systems (as required by Fig. 10), with both required $\log \Delta E$ and $(\log \mathrm{P})/(\log P_{\mathrm{mech}})$ showing a weakly significant tendency to increase with T, at $\sigma_{\mathrm{K}} = +1.4$ and $\sigma_{\mathrm{K}} = +1.6$, respectively.

5 PREHEATING AND METAL EJECTION FROM FEEDER FILAMENTS

The discussion in the preceding section focused on explaining the low IMLR in groups in the framework of a decreased potential for *in situ* metal production/release or retention in present-day group-sized haloes. Motivated by the limited success of these explanations, with the possible exception of AGN feedback, we now consider the possibility that it is mainly related to processes occurring at the epoch of galaxy formation. For example, the AGN results in Section 4.4 demonstrate that substantial, although not necessarily prohibitive, amounts of energy need to be injected into the ICM to accomplish the necessary gas and metal removal at low redshift from these groups. It would, however, have been energetically favourable to remove some of this material at a much earlier stage, when potential wells were shallower, and the gas more tenuous and likely exhibiting a more irregular geometry much more conducive to gas removal. It seems attractive to connect this possibility with the result that both SF and AGN activity were much stronger at high redshift, both peaking around $z \sim 2$–3 (Bouwens et al. 2007; Hopkins, Richards & Hernquist 2007). This section summarizes evidence that a significant fraction of metals in groups must have been generated before or during this phase, and discusses to what extent proto-galactic winds may have heated and dispersed this material beyond what is now r_{500}.

5.1 The case for early enrichment

There is substantial evidence that a significant fraction of the present-day metals in the Universe must have been generated at very early epochs. Enrichment of the intergalactic medium was taking place already at $z \sim 6$ (Simcoe 2006), with a non-negligible component of the produced metals residing in Lyman break galaxies, some of which presumably evolved into the massive cluster ellipticals seen today. Contenders for this early enrichment include proto-galactic winds occurring when (what are now) massive early-type galaxies formed the bulk of their stellar mass. In galaxy clusters, evidence for substantial enrichment prior to cluster collapse has been reported on the basis of measured large-radius abundances (Fujita et al. 2008). More generally, results for large cluster samples indicate that the hot gas had achieved a mean Fe abundance of $Z_{\mathrm{Fe}} \approx 0.3\,\mathrm{Z}_{\odot}$ by $z \sim 1$, comparable to that seen in nearby clusters, although some evolution in the central Fe content has occurred since then (Balestra et al. 2007; Maughan et al. 2008). The latter result draws support from the simulations of Cora et al. (2008), which suggest that cluster ICM abundances at large radii ($\sim r_{500}$) were largely established at $z \gtrsim 1$, with only central abundances increasing significantly since then. In smaller systems, the situation may be less clear (Finoguenov et al. 2002) but in the specific case of our groups, a couple of results do suggest that the material in their outskirts was predominantly enriched at early epochs by core-collapse SNe, whereas the abundance excesses in group cores may have been generated more recently.

First, the inferred number ratio of SN Ia to core-collapse SN in group cores of $\approx$0.4 is consistent with that measured in the local ($z \lesssim 0.7$) Universe in the *Hubble* and *Chandra* Deep Fields, but disagrees with predictions at $z \gtrsim 1$ for reasonable evolutionary models (Dahlen et al. 2004). In the absence of serious recent gas mixing (supported by the relatively undisturbed X-ray morphology and the pronounced Fe gradients of our groups), this suggests that the SN Ia-dominated group cores in general, and the central Fe and Si excesses in particular, have been generated within the last $\sim$5–7 Gyr. The abundance pattern seen in the heavily SN II-dominated outskirts which represent most of the ICM is, on the other hand, consistent with expectations for the SN Ia/SN II ratio at redshifts $z \gtrsim 1$ (Dahlen et al. 2004). Hence, most of the SN II activity in these groups likely took place at high redshift. This is in accordance with the result that most of our groups show a galaxy morphology–density relation of comparable strength to that observed in clusters (Helsdon & Ponman 2003), suggesting that SF and hence SN II activity has largely ceased at present in many of the bright galaxies in the central regions.

Second, even when allowing for enrichment through stellar mass loss from the central early type in each group, the discussion in Section 3.3 shows that an abundance contribution from SN II is, on average, required *everywhere* inside r_{500}. The near-uniform distribution of SN II products revealed by Fig. 6 suggests either an earlier enrichment epoch for these than for the SN Ia ejecta, allowing time for substantial mixing before and during group collapse, or a much more efficient redistribution mechanism for SN II ejecta. However, the results of Ferrara, Pettini & Shchekinov (2000) suggest that the distribution of SN II products in the absence of other mixing mechanisms should roughly follow that of the galaxy light. While this is observed for the central SN Ia products in at least some of our groups (Mendel et al. 2009), the SN II metals seem to trace more closely the much more extended distribution of the hot gas. The idea that SN II enrichment largely occurred before group/cluster collapse, as advocated by, for example, Finoguenov et al. (2001), implies that the

metals seen in group outskirts must have been generated by SN II before a significant number of SN Ia began exploding. Depending on the exact delay time distribution of SN Ia, this would imply SN II iron enrichment to a level of $\sim 0.1\,Z_{\odot}$ (Fig. 6) at redshifts $z \gtrsim 2$–3. As discussed earlier, the gentle central rise seen for SN II products can then be explained if a relatively small fraction of these metals were released after the group collapsed, possibly facilitated by galaxy–galaxy and galaxy–ICM interactions, and with an additional contribution associated with stellar wind loss from the central early-type galaxy.

By considering the typical time-scales for metal production in the groups, an additional argument can be provided in support of a prominent high-redshift contribution to ICM enrichment. For this, we focus first on the Fe produced by SN Ia, which is less likely than SN II products to become locked up in stars in the early-type galaxies that dominate the *K*-band output in our groups. Using the same general approach as for Fig. 12, while assuming a constant SN Ia rate per unit $L_{\rm K}$ equivalent to the value observed in local early types (Mannucci et al. 2005), we plot the resulting enrichment times corresponding to the total *K*-band $\mathrm{IMLR_{Ia}}$ within r_{500} in Fig. 19(a). Under these assumptions, the enrichment times should again be considered lower limits, because no account is made of metals locked in stars, metals that have left the group potential, or the growth of stellar mass within the group due to galaxy assembly, and the addition of galaxies to the group over the time-scales involved.

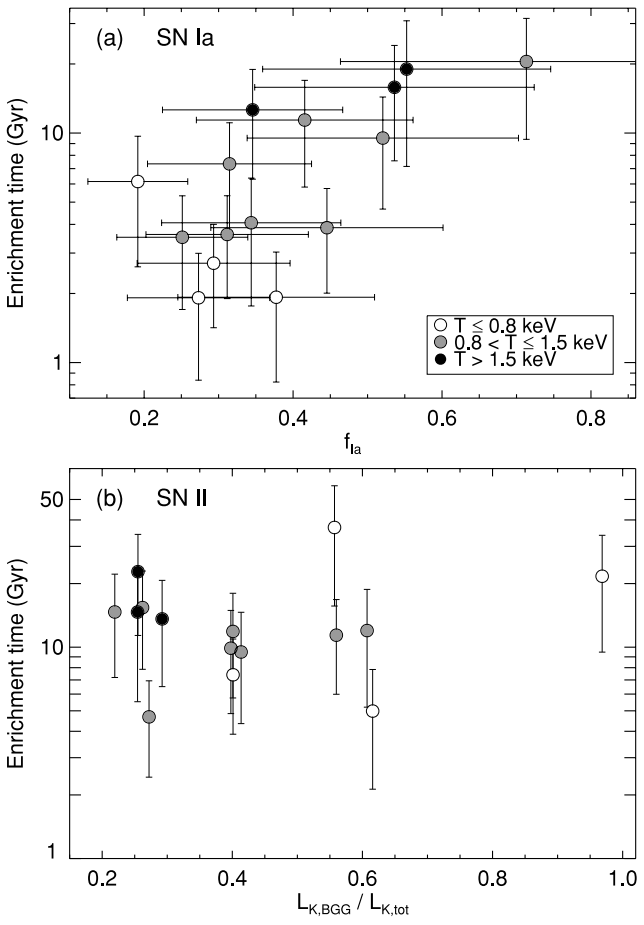

Figure 19. (a) SN Ia enrichment times based on the *K*-band $\mathrm{IMLR_{Ia}}$, plotted against the fractional Fe mass from SN Ia. (b) Similar for SN II, assuming local Sbc/d SN II rates for all satellite galaxies, as a function of the BGG contribution to total *K*-band light.

With results suggesting time-scales of $\gtrsim$10 Gyr in 40 per cent of our groups, typically in the hotter and more SN Ia-dominated ones, it is far from clear that specific SN Ia rates seen in present-day early types can account for the observed metal masses. The discussion in previous sections further indicates that contributions from stellar mass loss and IC stars are insufficient for bringing these time-scales below $\sim$10 Gyr in all groups; either the specific SN Ia rate must increase with redshift, or 'external' enrichment must be invoked to explain the observed amount of Fe from SN Ia.

This issue is even more acute for SN II, whose contribution to Fe enrichment is globally at least as important as that of SN Ia (cf. Table 1), but for which only upper limits to the observed rate in local early-types are available (Mannucci et al. 2005). These generally imply enrichment times far in excess of the age of the Universe. However, some morphological transformations and truncation of SF has likely taken place in the group members (Helsdon & Ponman 2003), so assuming current early-type SN II rates could well underestimate the metal output over cosmic time. In a crude attempt to correct for this, we employ the conservative assumption that all stellar mass not currently in the BGG has produced SN II according to the rate in local late-type *spirals*. The result is shown in Fig. 19(b). As is clear, time-scales are still prohibitively large in several cases, implying that SN II rates must also evolve with redshift, and even more so than for SN Ia. Specific SFRs, and hence metal production rates, must have been considerably higher in the past in these groups. Though not a surprising result, it lends independent support to the notion that an important fraction of ICM metals within r_{500} was generated at early epochs.

5.2 Linking enrichment to preheating

With much of the ICM pollution likely taking place around $z \sim$ 2–3, close to the redshift peaks of the cosmic SFR and of the AGN luminosity density, it is conceivable that metals and energy were released from galaxies in substantial amounts before gas and galaxies collapsed into groups, i.e. while still located in filaments of low overdensities. This would not only suggest that the trends in Fig. 8 were at least partly established at this epoch, but also offer a possible explanation of their origin in gas and metal loss from the filaments that fed the growth of the group structures observed today. Accretion along filaments implies, unlike the case for virialized structures, a preferred direction along which the ejection and loss of galactic material is strongly favoured. Given the available data, we can only make some general speculations about this possibility, but it seems an attractive one in light of the somewhat limited success of the other explanations considered.

ICM enrichment at high redshift could possibly be linked to the putative 'preheating' invoked in some models, by which the ICM in these systems is assumed to have had its entropy raised at high redshift in order to explain the similarity breaking in the X-ray scaling properties of groups and clusters. Simulations and observations (Borgani et al. 2008a and references therein) indicate that the associated energy required is of order $\sim$1 keV per particle, depending on the exact redshift of energy injection. It cannot greatly exceed this value, as preheating would otherwise have destroyed the ICM in $T \lesssim 1$ keV groups. While the initial argument for introducing this was to explain the seemingly elevated entropy levels in group cores, preheating could also affect the gas at larger radii. For example, the low gas mass-to-light ratio within r_{500} in cool systems could be related to the possibility that groups have

seriously inflated ICM distributions as a consequence of preheating through early galactic winds. The resulting entropy of the heated (and possibly enriched) gas would make it more resilient to gravitational compression, to a certain extent preventing its re-collapse into the group structures seen at low redshift. This is somewhat akin to the 'preferential infall' scenario proposed by Finoguenov et al. (2001), in which small groups preferentially accrete low-entropy, low-metallicity gas that was only mildly heated at high redshift.

One implication would be that a relatively larger fraction of any gravitationally bound X-ray gas and metals should reside beyond r_{500} in cooler systems. We are not in an optimal position to test this, as it would require sensitive X-ray data extending beyond this radius for all groups. We can only note that with the adopted density parametrizations, the ratio of gas mass within $0.5r_{500}$ to that within $0.5-1r_{500}$ actually shows a weak *anti*-correlation with $\langle T\rangle$ ($\sigma_{\rm K} = -1.6$) for our groups, consistent with the correlation seen between β and T for the GEMS sample in general ($\sigma = -1.4$; Osmond & Ponman 2004), from which the majority of our groups were selected. However, Sanderson & Ponman (2003) do find a positive dependence of β on T when including clusters in the comparison. The group–cluster discrepancy within r_{500} could contain some contribution from this effect, and if so would suggest that a more fair comparison of systems across a wide range of masses should be conducted within radii of lower overdensity such as r_{200}.

Our speculation that a considerable fraction of the (centrally concentrated) SN Ia products were released after group collapse suggests that at least part of the enrichment is not associated with preheating but must have occurred at later times at $z \lesssim 1$. This agrees with the conclusion of Finoguenov et al. (2002), based on the absence of a correlation between entropy at radii of equal enclosed mass versus Fe or Si abundance across a wide range of system masses. However, SN II provide the clear majority of the estimated SN energy released in our groups, with an average contribution to $E_{\rm SN,*}$ in Fig. 15 of $\approx$0.8 keV per particle, most of which was presumably released in early starbursts prior to group collapse. A potential caveat to the assumption that this value also corresponds to the energy *delivered* to the ICM by galaxies is that much of the SN explosion energy may have been rapidly radiated away in the initial starburst phase rather than released from galaxies in kinetic form. Whereas radiative losses are presumed to be minor at low redshift, with direct escape of the SN explosion energy facilitated by the presence of bubbles and chimneys in the ISM carved out by previous generations of SN (and winds from their progenitors), the ISM was denser, colder, and less porous at high redshift, possibly enhancing radiative losses. If so, the $\approx$0.8 keV per particle inferred from the stellar mass of the group members may represent an upper limit to the actual SN II energy delivered to the galaxy surroundings. On the other hand, simulations (Strickland & Stevens 2000) indicate that coordinated SN explosions, such as those likely taking place during vigorous high-redshift starbursts, tend to lower radiative losses. Furthermore, Fig. 15 suggests that the estimated SN energy associated with the ICM metal mass broadly matches the 'available' energy, so any overestimation of the SN energy imparted to the ICM should be modest.

Even if only a minor fraction of this energy were actually delivered to the surroundings in proto-galactic winds, it could still have contributed substantially to pre-heating the filaments feeding group formation. It may not be sufficient to entirely explain the similarity breaking between groups and clusters, or the presence of an 'entropy ramp' in group and cluster cores, but it certainly eases the energetic requirements imposed on any other source to deliver the remaining heating, and it may leave limited scope for AGN feedback. In the cluster regime, numerical simulations (Tornatore et al. 2004) suggest that a feedback mechanism not associated with SN has to be acting at early stages of cluster formation, before most of the mass is accreted in the cluster potential well, in order to avoid the centrally peaked Fe distribution seen in some simulations. At lower masses, however, where our results show stronger Fe gradients that in clusters, the need for AGN feedback is perhaps less pressing. The simulation work of Davé et al. (2008), for example, indicates that elevated entropy levels in groups may be largely explained by radiative cooling combined with SN-driven outflows, with no strong need for AGN-driven preheating.

Regardless of the heating source, the energetic requirements for blow-out of gas via buoyancy discussed in Section 4.4 would be strongly relaxed if the surrounding material is at a lower overdensity than currently seen in group cores. For example, Fig. 18 is based on assuming current ICM densities within $\sim$10–20 kpc of the group cores, which generally translate into cosmic overdensities of order $\sim 10^3$. If the gas to be heated has lower overdensities by a factor of $\sim$100 (certainly realistic for pre-virialized structures such as inflowing filaments), the requirements for heating it to current entropies at r_{500} would be reduced by a factor of $\sim$20, i.e. to just $\sim$0.1 keV particle^{-1} on average. This should be within range of *either* SN or AGN at $z \sim 2-3$, suggesting that the energy required to drive metals out of filaments is, indeed, available.

Whether the balance between bulk gas loss and selective loss of both SN Ia and SN II products suggested by our results can be achieved is a non-trivial question though. The shortfall of SN II products in groups seems largely explicable on the basis of pre-collapse metal loss in starburst winds, but removal of large amounts of Fe from SN Ia at early epochs may also require some of this material to have been synthesized very rapidly, for example by a population of SN Ia exploding promptly after SF. The existence of such a population has been proposed by Mannucci, Della Valle & Panagia (2006) on the basis of observed SN Ia rates at high redshift, but the need for this population at early times is still debated (Dahlen, Strolger & Riess 2008). Nevertheless, even in the 'standard' SN Ia delay time scenario, a non-negligible fraction of SN Ia products may have been released at fairly high redshift. For example, the model of Cora (2006) predicts a peak in the SN Ia iron injection rate at $z \sim 2$–3 in satellite galaxies and even earlier in the central galaxy.

While some SN Ia material *may* thus have been ejected from cool systems in early starburst winds, our discussion of Fig. 6, which shows that the SN Ia contribution becomes insignificant outside $\sim 0.7r_{500}$ still argues against a significant pre-collapse SN Ia contribution and so against substantial loss of SN Ia metals from filaments. To explore this issue further, we plot in Fig. 20 Fe masses from SN Ia within different radial intervals, all simply normalized by total stellar light $L_{\rm K}$. The plot suggests that, over the mass range considered here, the reduction in $\mathrm{IMLR_{Ia}}$ in lower mass systems has preferentially occurred within the central group regions, with no trend with $\langle T\rangle$ seen beyond $0.5r_{500}$. This preferential loss of SN Ia products from the central Fe peak seems consistent with post-collapse AGN outflows (and possibly some cooling) as important contributors to the shortfall of SN Ia products in cool systems. The considerations in Section 4.4.2 then suggest that this loss cannot generally have occurred very recently but rather must have taken place over considerable time-scales following group collapse.

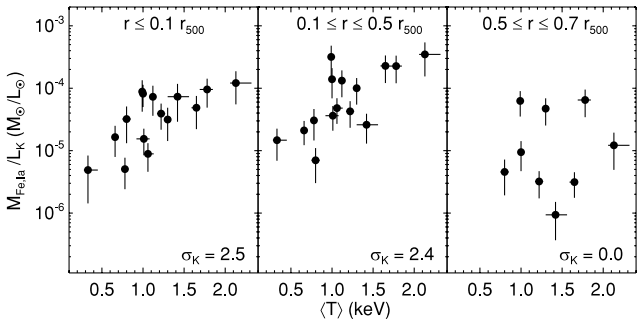

Figure 20. Mass of Fe from SN Ia within different radial ranges, normalized by total L_K. As in Fig. 10, only groups with data covering the full radial interval are shown in each panel. Labels in lower right corners specify the significance σ_K of any linear correlation.

6 DISCUSSION AND CONCLUSIONS

Based on the results presented in Paper I in this series (Rasmussen & Ponman 2007), in this second of two papers we have investigated the distribution and total mass of SN Ia and SN II products in the ICM of 15 groups, for comparison to the total ICM mass and to the optical luminosities and stellar masses of the group members. We re-emphasize here that our group sample was not intended to be statistically representative in any sense. Nevertheless, the results should still provide useful constraints on models of the evolution of galactic systems on scales from small groups to massive clusters. We note that there are features of the observed abundance distributions that we have not covered in any detail. These include the broad extent of the central abundance excess, reaching well beyond the distribution of stellar light from the central galaxy, as well as the curious abundance dips seen for both Fe and Si at the very centre for several groups, manifest also in the averaged profiles in Fig. 1. Any detailed discussion of these features is likely to benefit from comparison of group properties to those of non-cool-core systems, however, and so is deferred to a future paper. Our existing results can be summarized as follows:

(1) As anticipated, the total mass of iron and silicon in the hot gas within r_{500} scales strongly with total group mass as measured by the mean X-ray temperature outside any cool core. Values range from $M_{\rm Fe} = (0.4\text{–}23) \times 10^8\,{\rm M}_\odot$ and $M_{\rm Si} = (0.6 - 35) \times 10^8\,{\rm M}_\odot$ across the 0.3–2.1 keV temperature range of the sample. SN II have provided on average ∼60 per cent of the Fe and ∼90 per cent of the Si inside r_{500}, with a mildly significant tendency (at $\leq 2\sigma$) towards increasing SN II dominance in cooler systems.

(2) For the sample as a whole, the distribution of SN Ia products is strongly peaked towards the group core, whereas SN II enrichment is nearly uniform throughout the ICM. The Fe mass within $0.1r_{500}$ (roughly the size of the cool core, where present) can be explained by prolonged enrichment by SN Ia in the central early-type galaxy, aided by stellar mass loss and IC stars. In particular, if adopting a plausible model for the cosmic evolution of the SN Ia rate, typical enrichment time-scales are $\lesssim$5–7 Gyr in all groups, comparable to similar results for central cluster galaxies. The mild central rise observed for SN II products can be explained by stellar mass loss from the central galaxy, potentially with an additional contribution from metals released by other group galaxies via density-dependent release mechanisms such as galaxy–ICM interactions.

(3) Due to the combination of lower gas mass-to-light ratios and metal abundances in cooler systems, resulting aggregate metal mass-to-light ratios within r_{500} show an order-of-magnitude variation across the sample, only approaching results for massive clusters at the high-temperature end. For a given amount of stellar light, there is thus a substantial shortfall of X-ray metals in cooler systems, a deficiency which is found to be present both for SN Ia and SN II products. This suggests that metals from both SN types were either synthesized or released from galaxies less efficiently in lower mass systems, that metals were lost from such systems, or that the intergalactic gas accreted by small groups was less enriched than that accreted by more massive systems

(4) Both Fe and Si abundances in group cores ($r \lesssim 0.3r_{500}$) show a positive trend with group temperature which is significant at $\sim 3\sigma$. No corresponding trend is seen at larger radii ($r \gtrsim 0.5r_{500}$) however, arguing against recent preferential loss of enriched material from cooler systems as an explanation of their lower global metal-mass-to-light ratios. Estimates of the current mechanical power of the central AGN in the groups indicate that the metallicity trend in group cores may at least be partly due to the expulsion of enriched material to beyond $0.1r_{500}$ by AGN-driven buoyant bubbles, perhaps with some contribution from radiative cooling of enriched gas in the core, causing less enriched material to flow inwards. Alternatively, it can be understood as due to the action of a metal release mechanism whose efficiency depends on local ICM density and the total mass of the system, such as ram pressure stripping, but it cannot be explained by a systematic variation in the contribution from IC stars with group temperature. The absence of a similar reported trend in systems above $T \approx 2$ keV may indicate that the relevant processes 'saturate' in cluster cores, perhaps as a consequence of near-complete gas removal from core galaxies in such environments, or due to the larger heating energies or time-scales required to accomplish significant metal removal by AGN outflows or radiative cooling in such systems.

(5) As a consequence of the lower Fe abundances and mildly increased contribution from SN II in cooler systems (i.e. higher α/Fe ratios), we find tentative evidence for the ICM within the central few hundred kpc ($r \lesssim 0.5r_{500}$) to appear chemically less 'evolved' in these groups. This may reflect a more extended SF history in less massive groups, consistent with the slightly bluer average galaxy colour seen in these systems.

(6) Metal release from galaxies to the ICM appears to have been efficient in these groups with, on average, an estimated ∼70 per cent of the metals synthesized in galaxies currently present in the ICM. While this is in fair agreement with recent independent estimates in clusters (Sivanandam et al. 2009), there is also some evidence for the release fraction to be systematically lower, and well below cluster values, in the cooler groups in our sample.

(7) Among possible explanations for the metal deficiency in groups within r_{500}, we can rule out radiative cooling as an important gas and metal sink. Some contribution may instead come from the more extended SF histories and lower metal release efficiencies in cooler systems, as well as the tendency for such systems to contain a relatively larger fraction of their gas beyond r_{500}. Within the current ICM configuration, the energetic requirements for the necessary gas and metal loss induced by AGN- or SN-driven winds are rather large (although not necessarily prohibitively so), generally favouring loss of material at the incipient stages of group evolution. Other mechanisms such as thermal conduction transporting gas and metals out beyond r_{500} in cooler systems can probably be ruled out, due to the strong temperature dependence anticipated for heat conduction unsuppressed by magnetic fields (Spitzer conductivity $\propto T^{5/2}$).

(8) Comparison to observed ratios of SN Ia to core-collapse SN in deep field data (Dahlen et al. 2004) shows that group cores display

abundance ratios consistent with inferred SN ratios in the low-redshift Universe ($z \lesssim 0.7$), but are inconsistent with predictions for $z \gtrsim 1$. This argues in favour of relatively recent enrichment of the central group regions, including the build-up of the central abundance excesses over the past $\lesssim$6–8 Gyr. In contrast, the heavily SN II-dominated abundance ratios in group outskirts does agree with predictions for $z \gtrsim 1$, suggesting that most of the ICM was enriched to $\sim$0.1 solar at redshifts close to the peak of the cosmic SFR . The near-uniform radial distribution of SN II products corroborates this picture by arguing in favour of substantial SN II enrichment prior to or during group collapse.

(9) This raises the possibility that powerful starburst winds at high redshift have contributed significantly to the gas and metal deficiency in groups, causing loss of baryons from the filaments feeding the growth of these structures. The estimated SN explosion energy associated with high-z SF in the group members seems sufficient for this, and may further have provided a substantial fraction of the preheating energy required by some models for explaining the X-ray scaling properties of groups. If so, it is not clear that a prominent contribution to preheating from quasar activity is required in these systems. Post-collapse AGN feedback can nevertheless still have played a prominent role in subsequently ejecting mainly SN Ia metals from group potentials.

One implication of our results is that present-day clusters cannot have formed through hierarchical build-up of smaller structures resembling the groups studied here. This is, of course, already clear from the well-established differences in cold fraction (cf. Section 4.1), but the deficiency of gas-phase metals in smaller systems poses an additional problem for this scenario. Of course there is no compelling reason to believe that present-day groups are chemically similar to those that participated in cluster build-up at higher redshift, although our considerations suggest that the metal deficiency in low-mass systems has not been established recently. Alternatively, the proto-clusters into which such groups merged have been massive enough to retain or re-accrete enriched material shed by their smaller progenitors. Deep X-ray observations of high-z groups may eventually shed light on these issues, but the questions are unlikely to be settled by the current generation of X-ray satellites. Numerical work may also provide clues to the chemical properties of cluster progenitors and in which ways these depart from those of our groups. A prerequisite for such a comparison, however, is that models can accurately reproduce observational results for the ICM abundance distribution in groups at low redshift. While significant improvements have been made in the past few years in this regard, some issues remain such as reproducing the observed distribution of α-elements (see e.g. Davé et al. 2008).

Alternatively, our groups are conceivably not representative of (X-ray) groups in general. Although exhibiting X-ray luminosities that span two orders of magnitude (Osmond & Ponman 2004), our group sample is still largely restricted to cool-core groups that appear morphologically undisturbed. In order to gain a more complete picture of the enrichment and feedback history in groups, similar analyses would need to be extended to a more heterogeneous group sample, including a substantial number of systems without a cool core. At higher masses, such systems tend to show much flatter abundance gradients than those reported here (e.g. De Grandi et al. 2004), suggesting fundamental differences in ICM enrichment and heating histories between cool-core and non-cool-core systems. Such a comparison is the subject of ongoing work (Johnson et al., in preparation), and may ultimately help in providing an improved understanding of the chemical and thermodynamical evolution of baryons in both galaxies and the intergalactic medium.

ACKNOWLEDGMENTS

We are grateful to the referee for helpful and constructive comments which helped to clarify the robustness of our conclusions. We acknowledge useful discussions with Alexis Finoguenov, Alastair Sanderson and François Schweizer. This work has made use of the NASA/IPAC Extragalactic Data base (NED) and the Two-Micron All-Sky Survey (2MASS) data base. JR acknowledges support provided by the National Aeronautics and Space Administration through Chandra Postdoctoral Fellowship Award Number PF7-80050 issued by the Chandra X-ray Observatory Center, which is operated by the Smithsonian Astrophysical Observatory for and on behalf of the National Aeronautics and Space Administration under contract NAS8-03060.

REFERENCES

Allen S. W., Dunn R. J. H., Fabian A. C., Taylor G. B., Reynolds C. S., 2006, MNRAS, 372, 21
Arav N. et al., 2007, ApJ, 658, 829
Baldi A., Ettori S., Mazzotta P., Tozzi P., Borgani S., 2007, ApJ, 666, 835
Balestra I., Tozzi P., Ettori S., Rosati P., Borgani S., Mainieri V., Norman C., Viola M., 2007, A&A, 462, 429
Baumgartner W. H., Loewenstein M., Horner D. J., Mushotzky R. F., 2005, ApJ, 620, 680
Bell E. F., de Jong R. S., 2001, ApJ, 550, 212
Bernardi M. et al., 2003, AJ, 125, 1882
Bîrzan L., Rafferty D. A., McNamara B. R., Wise M. W., Nulsen P. E. J., 2004, ApJ, 607, 800
Borgani S. et al., 2004, MNRAS, 348, 1078
Borgani S., Diaferio A., Dolag K., Schindler S., 2008a, Space Sci. Rev., 134, 269
Borgani S., Fabjan D., Tornatore L., Schindler S., Dolag K., Diaferio A., 2008b, Space Sci. Rev., 134, 379
Böhringer H., Matsushita K., Churazov E., Finoguenov A., Ikebe Y., 2004, A&A, 416, L21
Bouwens R. J., Illingworth G. D., Franx M., Ford H., 2007, ApJ, 670, 928
Bower R. G., McCarthy I. G., Benson A. J., 2008, MNRAS, 390, 1399
Brinchmann J., Charlot S., White S. D. M., Tremonti C., Kauffmann G., Heckman T., Brinkmann J., 2004, MNRAS, 351, 1151
Brough S., Proctor R., Forbes D. A., Couch W. J., Collins C. A., Burke D. J., Mann R. G., 2007, MNRAS, 378, 1507
Buote D. A., 2000a, MNRAS, 311, 176
Buote D. A., 2000b, ApJ, 539, 172
Buote D. A., Brighenti F., Mathews W. G., 2004, ApJ, 607, L91
Capetti A., Verdoes Kleijn G., Chiaberge M., 2005, A&A, 439, 935
Cattaneo A., Dekel A., Faber S. M., Guiderdoni B., 2008, MNRAS, 389, 567
Ciotti L., D'Ercole A., Pellegrini S., Renzini A., 1991, ApJ, 376, 380
Combes F., Young L. M., Bureau M., 2007, MNRAS, 377, 1795
Conroy C., Wechsler R. H., Kravtsov A. V., 2007, ApJ, 668, 826
Cora S. A., 2006, MNRAS, 368, 1540
Cora S. A., Tornatore L., Tozzi P., Dolag K., 2008, MNRAS, 386, 96
Cox T. J., Di Matteo T., Hernquist L., Hopkins P. F., Robertson B., Springel V., 2006, ApJ, 643, 692
De Grandi S., Ettori S., Longhetti M., Molendi S., 2004, A&A, 419, 7
Dahlen T. et al., 2004, ApJ, 613, 189
Dahlen T., Strolger L.-G., Riess A. G., 2008, ApJ, 681, 462
Dale D. A. et al., 2007, ApJ, 655, 863
Davé R., Oppenheimer B. D., Sivanandam S., 2008, MNRAS, 391, 110
Davis D. S., Mulchaey J. S., Mushotzky R. F., Burstein D., 1996, ApJ, 460, 601

de Plaa J., Werner N., Bleeker J. A. M., Vink J., Kaastra J. S., Méndez M., 2007, A&A, 465, 345
Domainko W. et al., 2006, A&A, 452, 795
Ettori S., 2003, MMRAS, 344, L13
Ettori S., 2005, MNRAS, 362, 110
Ferrara A., Pettini M., Shchekinov Y., 2000, MNRAS, 319, 539
Ferrarese L., Merritt D., 2000, ApJ, 539, L9
Finoguenov A., Ponman T. J., 1999, MNRAS, 305, 325
Finoguenov A., David L. P., Ponman T. J., 2000, ApJ, 544, 188
Finoguenov A., Arnaud M., David L. P., 2001, ApJ, 555, 191
Finoguenov A., Jones C., Böhringer H., Ponman T. J., 2002, ApJ, 578, 74
Finoguenov A., Burkert A., Böhringer H., 2003, ApJ, 594, 136
Finoguenov A., Davis D. S., Zimer M., Mulchaey J. S., 2006, ApJ, 646. 143
Finoguenov A., Ponman T. J., Osmond J. P. F., Zimer M., 2007, MNRAS, 374, 737
Fujita Y., Tawa N., Hayashida K., Takizawa M., Matsumoto H., Okabe N., Reiprich T. H., 2008, PASJ, 60, 343
Gastaldello F., Buote D. A., Humphrey P. J., Zappacosta L., Bullock J. S., Brighenti F., Mathews W. G., 2007, ApJ, 669, 158
Gastaldello F., Buote D. A., Temi P., Brighenti F., Mathews W. G., Ettori S., 2009, ApJ, 693, 43
Gebhardt K. et al., 2000, ApJ, 539, L13
Gibson B. K., Loewenstein M., Mushotzky R. F., 1997, MNRAS, 290, 623
Gonzalez A. H., Zaritsky D., Zabludoff A. I., 2007, ApJ, 666, 147
Grevesse N., Sauval A. J., 1998, Space Sci. Rev., 85, 161
Helsdon S. F., Ponman T. J., 2000, MNRAS, 319, 933
Helsdon S. F., Ponman T. J., 2003, MNRAS, 340, 485
Hopkins P. F., Hernquist L., Cox T. J., Di Matteo T., Robertson B., Springel V., 2006, ApJS, 163, 1
Hopkins P. F., Richards G. T., Hernquist L., 2007, ApJ, 654, 731
Humphrey P. J., Buote D. A., 2006, ApJ, 639, 136
Iwamoto K., Brachwitz F., Nomoto K., Kishimoto N., Umeda H., Hix W. R., Thielemann F.-K., 1999, ApJS, 125, 439
Jetha N. N., Hardcastle M. J., Babul A., O'Sullivan E., Ponman T. J., Raychaudhury S., Vrtilek J., 2008, MNRAS, 384, 1344
Kapferer W. et al., 2007, A&A, 466, 813
Kennicutt R. C. Jr., 1998, ARA&A 36, 189
Komiyama M., Sato K., Nagino R., Ohashi T., Matsushita K., 2009, PASJ, 61, 337
Leccardi A., Molendi S., 2008, A&A, 487, 461
Lin Y.-T., Mohr J. J., 2004, ApJ, 617, 879
Lin Y.-T., Mohr J. J., Stanford S. A., 2003, ApJ, 591, 749
Lin Y.-T., Mohr J. J., Stanford S. A., 2004, ApJ, 610, 745
Loewenstein M., 2006, ApJ, 648, 230
McNamara B. R., Nulsen P. E. J., 2007, ARA&A, 45, 117
Mannucci F., Della Valle M., Panagia N., Cappellaro E., Cresci G., Maiolino R., Petrosian A., Turatto M., 2005, A&A, 433, 807
Mannucci F., Della Valle M., Panagia N., 2006, MNRAS, 370, 773
Maughan B. J., Jones C., Forman W., Van Speybroeck L., 2008, ApJS, 174, 117
Mendel T. J., Proctor R. N., Rasmussen J., Forbes D. A., Brough S., 2009, MNRAS, 396, 2103
Merloni A., Heinz S., 2008, MNRAS, 388, 1011
Moll R. et al., 2007, A&A, 463, 513
Morita U., Ishisaki Y., Yamasaki N. Y., Ota N., Kawano N., Fukazawa Y., Ohashi T., 2006, PASJ, 58, 719
Mouhcine M., Bamford S. P., Aragón-Salamanca A., Nakamura O., Milvang-Jensen B., 2006, MNRAS, 368, 1871
Mulchaey J. S., Davis D. S., Mushotzky R. F., Burstein D., 2003, ApJS, 145, 39
Navarro J. F., Frenk C. S., White S. D. M., 1997, ApJ, 490, 493
Nomoto K., Tominaga N., Umeda H., Kobayashi C., Maeda K., 2006, Nucl. Phys. A, 777, 424
Osmond J. P. F., Ponman T. J., 2004, MNRAS, 350, 1511
Ponman T. J., Sanderson A. J. R., Finoguenov A., 2003, MNRAS, 343, 331
Purcell C. W., Bullock J. S., Zentner A. R., 2007, ApJ, 666, 20
Rafferty D. A., McNamara B. R., Nulsen P. E. J., Wise M. W., 2006, ApJ, 652, 216
Rasmussen J., Ponman T. J., 2004, MNRAS, 349, 722
Rasmussen J., Ponman T. J., 2007, MNRAS, 380, 1554 (Paper I)
Rasmussen J., Ponman T. J., Mulchaey J. S., 2006, MNRAS, 370, 453
Rebusco P., Churazov E., Böhringer H., Forman W., 2006, MNRAS, 372, 1840
Renzini A., 1997, ApJ, 488, 35
Renzini A., 2004, in Mulchaey J. S., Dressler A., Oemler A., eds, Clusters of Galaxies: Probes of Cosmological Structure and Galaxy Evolution. Cambridge Univ. Press, Cambridge, p. 260
Renzini A., Ciotti L., D'Ercole A., Pellegrini S., 1993, ApJ, 419, 52
Rifatto A., Longo G., Capaccioli M., 1995, A&AS, 114, 527
Roediger E., Brüggen M., Rebusco P., Böhringer H., Churazov E., 2007, MNRAS, 375, 15
Romeo A. D., Sommer-Larsen J., Portinari L., Antonuccio-Delogu V., 2006, MNRAS, 371, 548
Sánchez-Blázquez P., Gorgas J., Cardiel N., González J. J., 2006, A&A, 457, 809
Sánchez-Blázquez P., Forbes D. A., Strader J., Brodie J., Proctor R., 2007, MNRAS, 377, 759
Sanderson A. J. R., Ponman T. J., 2003, MNRAS, 345, 1241
Sanderson A. J. R., Ponman T. J., Finoguenov A., Lloyd-Davies E. J., Markevitch M., 2003, MNRAS, 340, 989
Sanderson A. J. R., Ponman T. J., O'Sullivan E., 2006, MNRAS, 372, 1496
Sato K., Tokoi K., Matsushita K., Ishisaki Y., Yamasaki N. Y., Ishida M., Ohashi T., 2007, ApJ, 667, L41
Sato K., Matsushita K., Ishisaki Y., Yamasaki N. Y., Ishida M., Ohashi T., 2009, PASJ, 61, 353
Sengupta C., Balasubramanyam R., 2006, MNRAS, 369, 360
Simcoe R. A., 2006, ApJ, 653, 977
Sivanandam S., Zabludoff A. I., Zaritsky D., Gonzalez A. H., Kelson D. D., 2009, ApJ, 691, 1787
Skrutskie M. F. et al., 2006, AJ, 131, 1163
Spolaor M., Forbes D. A., Proctor R. N., Hau G. K. T., Brough S., 2008, MNRAS, 385, 675
Spolaor M., Proctor R. N., Forbes D. A., Couch W. J., 2009, ApJ, 691, L138
Stott J. P., Edge A. C., Smith G. P., Swinbank A. M., Ebeling H., 2008, MNRAS, 384, 1502
Strickland D. K., Stevens I. R., 2000, MNRAS, 314, 511
Strickland D. K., Heckman T. M., Colbert E. J. M., Hoopes C. G., Weaver K. A., 2004, ApJS, 151, 193
Strolger L.-G. et al., 2004, ApJ, 613, 200
Sun M., Voit G. M., Donahue M., Jones C., Forman W., Vikhlinin A., 2009, ApJ, 693, 1142
Tamura T., Kaastra J. S., den Herder J. W. A., Bleeker J. A. M., Peterson J. R., 2004, A&A, 420, 135
Tokoi K. et al., 2008, PASJ, 60, 317
Tornatore L., Borgani S., Matteucci F., Recchi S., Tozzi P., 2004, MNRAS, 349, L19
Trentham N., Tully R. B., Mahdavi A., 2006, MNRAS, 369, 1375
Vikhlinin A., Kravtsov A., Forman W., Jones C., Markevitch M., Murray S. S., Van Speybroeck L., 2006, ApJ, 640, 691
Wang T.-G., Zhou H., Lu H., Yuan W., Shan H., Dong X., 2007, in Ho L., Wang J.-M., eds, ASP Conf. Ser. Vol. 373. The Central Engine of Active Galactic Nuclei. Astron. Soc. Pac., San Francisco, p. 331

This paper has been typeset from a TEX/LATEX file prepared by the author.